

See discussions, stats, and author profiles for this publication at: <https://www.researchgate.net/publication/320686586>

Global available wind energy with physical and energy return on investment constraints

Article in Applied Energy · October 2017

DOI: 10.1016/j.apenergy.2017.09.085

CITATIONS

130

3 authors:



Elise Dupont

Université Catholique de Louvain - UCLouvain

7 PUBLICATIONS 246 CITATIONS

[SEE PROFILE](#)

READS

15,153



Rembrandt Koppelaar

Imperial College London

42 PUBLICATIONS 976 CITATIONS

[SEE PROFILE](#)



Hervé Jeanmart

Université Catholique de Louvain - UCLouvain

138 PUBLICATIONS 2,899 CITATIONS

[SEE PROFILE](#)

Global Available Wind Energy with Physical and Energy Return on Investment Constraints

Elise Dupont^a, Rembrandt Koppelaar^{b,c}, Hervé Jeanmart^a

^a*iMMC - Institute of Mechanics, Materials and Civil Engineering, Université catholique de Louvain, 1348 Louvain-la-Neuve, Belgium*

^b*Centre for Environmental Policy, Faculty of Natural Science, Imperial College London, South Kensington Campus, London SW7 2AZ, England, UK*

^c*Institute for Integrated Economic Research, The Broadway W5 2NR, London*

Abstract

Looking ahead to 2050 many countries intend to utilise wind as a prominent energy source. Predicting a realistic maximum yield of onshore and offshore wind will play a key role in establishing what technology mix can be achieved, specifying investment needs and designing policy. Historically, studies of wind resources have however differed in their incorporation of physical limits, land availability and economic constraints, resulting in a wide range of harvesting potentials. To obtain a more reliable estimate, physical and economic limits must be taken into account.

We use a grid-cell approach to assess the theoretical wind potential in all geographic locations by considering technological and land-use constraints. An analysis is then performed where the Energy Return on Investment (EROI) of the wind potential is evaluated. Finally, a top-down limitation on kinetic energy available in the atmospheric boundary layer is imposed.

With these constraints wind farm designs are optimized in order to maximize the net energy flux. We find that the global wind potential is substantially lower than previously established when both physical limits and a high

cut-off EROI > 10 is applied. Several countries' potentials are below what is needed according to 100% renewable energy studies.

Keywords: Wind Energy, Electricity, Offshore Wind, Energy Return on Investment (EROI), Global Wind Potential, Net Energy

1. Introduction

Economic growth since the industrial revolution has been possible thanks to abundant sources of affordable energy, in the form of coal, oil and gas. However to mitigate climate change, we must urgently move away from fossil fuels. According to a study by McGlade and Ekins (2015) in Nature, a significant part of remaining fossil fuel reserves should remain unused in order to limit the increase in average global temperature to 2 °C. A rapid transition to a sustainable energy system is therefore the only option.

At the same time, energy demand will continue to increase significantly in the coming decades. According to some predictions it will reach 700-830 EJ by 2040 WEC (2016); IEA (2016), up to 550 EJ in 2015 BP (2016). Renewable energy sources therefore will not only have to substitute for fossil fuels but will also have to supply growing energy needs to support economic and population growth. Given these challenges it is essential to accurately take into account their future production potential in a low-carbon energy system.

Wind power achieves a prominent share in the power generation mix in many techno-economic future energy studies of countries and regions Walm-sley et al. (2014); Lunz et al. (2016); Zou et al. (2017). Without an evidence-based upper-bound based on geographic potential however, overestimates can

occur resulting in unrealistic transition scenarios. Moreover, with the pace of wind energy expansion being increasingly determined by government and companies via auctions, where capacities instead of prices are the fixed instrument of control, the provisioning of accurate long term capacity planning potential is even more important IRENA (2017).

A major challenge to impose realistic potentials in planning scenarios is the large discrepancy between studies on the global and regional wind energy potential (Table 1). The difference in wind potential estimates results in a wide range of possibilities for the future role of renewables. A large group of researchers evaluate that with the right policies we will be able to grow our level of consumption and support economic growth with a 100 % renewable energy system, thanks to technological progress, performance improvement, and cost reduction Jacobson and Delucchi (2011); WWF (2011); IRENA (2016); Jacobson et al. (2017).

Other authors are less optimistic, arguing that the renewable energy potential is overestimated and that the analysis of potential share includes significant uncertainties in physical requirements. They argue that key physical and geographic constraints, which limit energy availability and accessibility, have not been taken into account Mediavilla et al. (2013); Capellan-Perez et al. (2014); de Castro et al. (2011, 2013); Moriarty and Honnery (2012, 2016); Dale et al. (2012a,b).

In this study a novel methodology is described and implemented that to our knowledge is the first to combine physical, geographic, and economic constraints, derived from setting a minimum Energy Returned on Investment

(EROI) as a limiter to the harvestable wind resource. Thereby we gain a more precise value for the maximum offshore and onshore wind potential at a global and country level. These can be utilised to create more realistic future energy systems scenario studies to underpin policy decisions and investment need assessments.

In Section 2 key considerations to be taken into account in the analysis of wind energy potentials are discussed. They are followed by the methodology employed in this study in Section 3, results are presented in Section 4 and discussed in Section 5. Finally, the study ends with a set of conclusions and the implications for energy strategy policies in Section 6.

2. Background

2.1. Net Energy Availability

The field of net energy analysis studies the energy surplus available to society after subtracting input energy needed to construct and operate an energy supply chain. To account for energy available on a net basis, Net Energy Ratios, such as the Energy Return on Investment (EROI) or Energy Returned on Energy Invested (ERoEI), are calculated Dale et al. (2011, 2012a,b); Cleveland (2005); Mulder and Hagens (2008); Hall and Day (2009); Murphy et al. (2011); Murphy and Hall (2011); Murphy (2014) : these yield the ratio of energy delivered by an energy technology or system to the total amount of energy invested for its manufacture, transportation, construction, operation, maintenance, and decommissioning. This dimensionless factor enables a comparison between energy sources if the same boundaries for calculating inputs and outputs are used. First, it allows for an evaluation of the

energy made available to society net of the energy self-consumption of the sector itself, so as to assess - in an absolute manner - the net potential that energy technologies can deliver to the economy. Second, it allows to evaluate in energy transition scenarios how the scale of the energy sector would need to change to deliver the same or changing energy needs. For example, if the baseline EROI of the energy sector is 8 and if this is halved to 4 over time due to a switch to different energy technologies, this would result in a 2.3 times greater energy sector size to supply the same end energy service, and a drop from 8 to 2 implies a 7 times larger energy sector for the same end service. The weight of scaling in terms of the size of the energy sector versus the rest of the economy starts to matter at an EROI below 15 and becomes increasingly relevant as the value drops below 10. Because of this scaling effect, studies indicate that there is a minimum EROI value to maintain our current standard of living Hall et al. (2009, 2014); Lambert et al. (2014).

Static evaluations of EROI for a given energy technology are widely present in the literature Lenzen and Munksgaard (2002); Kubiszewski et al. (2010); Bhandari et al. (2015); Koppelaar (2017). However, few studies exist on the potential of technologies globally or regionally on a net energy basis, nor on the future evolution of EROI of renewable energy technologies and energy systems. As renewable resources and energy consumption are not equally distributed on earth, it is plausible that the EROI of renewable energy sources declines with spatial expansion Dale et al. (2011). Renewable energy projects will primarily be built on the best sites (i.e. the sites with the highest resources or that are close to end-users), subsequently, in order to significantly increase capacity, lower quality sites will have to be exploited.

So far few studies on renewable energy potentials take into account EROI dynamics, despite its importance to assess the feasibility to rapidly expand renewable energy technology in the future, except to the knowledge of the author's the work of Dale et al. (2012a,b) and Moriarty and Honnery (2011, 2012, 2016).

2.2. Maximum Wind Energy Potential

The amount of wind energy that is available at a global scale is constrained by physical factors including incoming solar radiation, heat gradient, geography, and electricity transport distance. A considerable number of studies estimate the technical potential of wind energy via a bottom-up approach neglecting energy conservation laws that are in effect at a global scale Hoogwijk (2004); Archer and Jacobson (2005); EEA (2009); Lu et al. (2009); Bosch et al. (2017); Eurek et al. (2017). Global potential is in these studies calculated from the sum of local potentials, based on the implicit assumption that the extraction of a large amount of wind power has no impact on global wind generation. However, wind power potential is not only limited by our ability to build and install more wind turbines, but also by the power generated by the sun. Therefore a global estimate of maximum kinetic energy extraction rates is needed, and should be taken into account as a physical constraint to the sum of local potentials.

In order to reach a significant contribution to the energy mix, wind farms will on average have to be composed of a substantial number of turbines. In very large wind farms, the horizontal flux of kinetic energy is captured by the first rows of turbines and can therefore be neglected. The power that can be captured is thus primarily limited by the vertical downward transport of

kinetic energy Meyers and Meneveau (2011).

On top of this limitation, global wind speeds will be reduced if a significant amount of wind power is extracted. A reduction in global wind speeds as a consequence of large scale wind turbine placement will potentially further reduce the energy produced by wind farms and likely have an impact on local and regional meteorology Abbasi et al. (2016). At present it is hard to picture that we could reach a level of wind energy production that could alter the global climate, but this is because wind energy extracted today still represents a small fraction of total wind energy available globally.

2.2.1. Literature estimates

In past decades several methods have been proposed to quantify limits on available energy from wind power generation.

Generation of kinetic energy. It has been shown that the conversion process of incident solar radiation into kinetic energy is currently maximal at a rate of 2%, corresponding to an available power flux of 900 TW globally Lorenz (1955, 1960); Gustavson (1979); Peixoto and Oort (1992); Kleidon (2010), with about a third dissipated within the surface boundary layer Hermann (2006). This gross estimation yields 292 TW kinetic energy dissipated in the atmospheric boundary layer. This value is consistent with results from other approaches: Jacobson and Archer (2012) found 253 TW for the saturation wind potential at 100 m and Miller and Kleidon (2016) found a dissipation rate of 270 TW via global circulation model (GCM) simulations.

Maximum extraction rates. Miller et al. (2011, 2012) studied maximum extraction rates for wind turbine technology, and by combining different ap-

proaches they found a 18-68 TW range for the wind energy potential, which equates to 567 to 2144 EJ/year. de Castro et al. (2013, 2011) studied the global wind energy potential with a top down approach based on the portion of kinetic energy that can be converted, with limitations of height, geography, wind turbines, economically viable areas, wind speeds, and conversion efficiency. The results yielded 1 TW as the global wind potential, which equates to 32 EJ/year. In comparison, total wind electricity production in 2016 was 3.5 EJ.

Gustavson (1979) estimated that the global limit for wind power extraction was 130 TW, assuming that up to 10 % of the near-surface dissipation of kinetic energy could be extracted.

Limits on power production density. Some studies use general circulation models or mesoscale models with wind turbine parametrization in order to predict climatic impacts of very large wind farms Keith et al. (2004); Miller et al. (2011); Jacobson and Archer (2012); Adams and Keith (2013). The analyses also have highlighted that by increasing the installed capacity density of wind farms the power produced saturates at capacity densities smaller than most current wind farms. Studies showed that for wind farms larger than 100 km² in windy regions (like the US Midwest and Western Europe) power production saturates at about 1 W_e/m² Miller et al. (2015); Adams and Keith (2013). This value was also found by Best (1978). Miller and Kleidon (2016) compared global circulation model simulations with estimates of vertical kinetic energy fluxes and found maximum electricity generation rates of 0.32 and 0.37 W_e/m² on land and 0.59 and 0.29 W_e/m² over oceans, with global wind speed reductions of 42 % and 44 %. Their results seem to con-

firm that few land areas are able to generate more than $1 \text{ W}_e/\text{m}^2$, and that large scale deployment would reduce the production of each turbine.

The results cited above which take into account physical limits to energy availability predict that it will be more difficult than anticipated for wind energy to contribute significantly to the world's energy needs.

The insights demonstrate that it is fundamental to combine a bottom-up with a top-down approach, so as to obtain a better estimate of the global wind energy potential. As a start we create and implement a novel bottom-up approach in this study, as outlined in Sections 3.1 and 3.4 which allows for an estimate of the energy generated in every geographic location, taking into account local constraints. We include in the analysis an assessment of energy inputs, as described in Sections 3.2 and 3.3, to ascertain how much energy output is available, net of inputs. The evaluation is subsequently adjusted with a constraint on the total available kinetic energy based on a simplified energy distribution model described in Section 3.5.

3. Methodology

Wind energy is one of the most promising sources to expand electricity generation in the future, but, as shown in Table 1, the range between estimates of its global potential is quite large. Given the ongoing scaling of wind turbine parks in the world to over a terawatt of capacity in the near-term, it is crucial to be able to refine these estimates with physical constraints to energy availability and accessibility.

To derive a more precise estimate of the global wind energy potential, the availability of wind energy is modelled on a net energy basis with a grid cell approach. The methodology is shown in Figure 1 and includes the following steps:

- **Bottom-up approach**

1. First a **suitability factor** is associated to each cell, as discussed in Section 3.1, in order to take into account geographical and technical constraints.
2. The theoretical **energy output** in each cell is evaluated as outlined in Section 3.2:
 - The **capacity factor** of a wind turbine is estimated, by combining wind speed distribution and turbine specifications (Section 3.2.1).
 - **The array placement efficiency** is then added (Section 3.2.2) in order to include wake effects of multiple turbines in geographic proximity.
3. Based on a detailed life-cycle inventory the **energy inputs** for a typical wind farm are evaluated in Section 3.3 (onshore, bottom-fixed offshore and floating offshore). The influence of distance to coast and water depth on energy inputs is incorporated.
4. An optimization procedure for the **installed capacity** is presented in Section 3.4, with the objective to find the maximum electricity generated on a net energy basis, using as a constraint a desired minimum EROI value.

- **Top-down approach**

5. A study of the **kinetic energy available** in the atmospheric boundary layer is made in Section 3.5. Energy conservation at a planetary scale is used as a constraint on the results from the bottom-up approach.

- **Results**

6. **The sustainable wind power potential** is calculated by adding constraints of step 5 to the optimization procedure of step 4 (Section 3.6). An upper limit to global wind power potential as a function of a minimum cut-off EROI is obtained.

The grid size of the model is $0.75^\circ \times 0.75^\circ$ ($4,000 \text{ km}^2$ on average), which corresponds to the smallest resolution available for wind speed data at hub height (71 and 124 m) in the ERA-Interim dataset Dee et al. (2011). As for land use types, the model resolution is $0.01^\circ \times 0.01^\circ$.

3.1. Geographic Suitability Factor

Since many areas are not suitable for wind farm installation, realistic assumptions should be taken regarding geographical constraints. Following the approach used in Hoogwijk (2004); Moriatry and Honnery (2011); Bosch et al. (2017); Eurek et al. (2017), a suitability factor is associated to each grid cell, defined as the cell fraction suitable for wind farm installation.

3.1.1. Onshore suitability factor

For onshore areas, the suitability factor depends on land cover. Values used in this study are given in Table 2, which are coherent with those in pre-

cited studies. Land cover of each grid cell was retrieved from the GlobCover 2009 dataset, created by the European Space Agency (ESA) and the Université catholique de Louvain (UCL) which classifies global land cover in 22 classes, at a 10 arc-second resolution ESA and UCL (2009). Because of the spatial area of the cells in our model ($\sim 4,000 \text{ km}^2$) it would be too coarse to associate a single land cover to an entire cell. Therefore, each $0.75^\circ \times 0.75^\circ$ grid cell was divided into a subgrid of $0.01^\circ \times 0.01^\circ$ subcells. By retrieving the land cover associated with the center of each subcell in the GlobCover dataset, the repartition of a cell's area into the 22 different land covers was estimated.

Bioreserves from the world database on protected areas IUCN and UNEP-WCMC (2016) are excluded, as well as relatively remote and unpopulated areas (Antarctica, Greenland and small remote islands). Countries for each grid cell are retrieved from VLIZ (2014).

3.1.2. Offshore suitability factor

Offshore areas are restricted to exclusive economic zones, i.e. sea zone up to 200 nautical miles from the coast (retrieved from VLIZ (2014)). Offshore wind energy potential and cost is dependent on water depth and distance to shore. Water depth will have an impact on the type of foundations since at greater depths pile based substructures are not possible. Current commercial substructures are limited to water depths of about 40 meters. In EEA (2009), the authors restricted offshore areas to sea depths below 50 meters. However, experimental floating substructures are in advanced stages of development and are expected to be adaptable for a wide range of water depths. Based on Smith et al. (2015), water depths up to 1000 m are allowed in the model.

Once the depth of offshore areas are set they are split according to the distance to the nearest coast. Assumptions and the resulting proportions of available area are summarised in Table 2. These values are based on the considerations found in EEA (2009); Smith et al. (2015) to take into account other uses of the sea area. For example, up to 5 nautical miles from the coast (about 10 km), wind turbines can be seen by the human eye and therefore their construction up to this distance is assumed to be limited to 10% of the area.

The combination of these constraints (protected areas, land-use, elevation, water depth, distance to shore) results in a calculated suitability factor for each grid cell, shown on a map in Figure 2.

3.2. Wind Energy Outputs

3.2.1. Capacity factor

The annual production of a wind turbine is obtained through an estimation of its capacity factor. The capacity factor is the ratio between the energy produced by a wind turbine over a period of time and the energy it would have produced if operating continuously at its nominal power rating during the same period, or equivalently it is the ratio of the mean power produced to its rated power. In most studies a linear relationship between capacity factor and mean wind speed at hub height is used. Here, instead of using mean wind speed we take into account wind speed distribution in order to obtain a more precise calculation Tian-Pau et al. (2014).

The capacity factor is calculated as follows:

$$C_f = \frac{\bar{P}}{P_r} = \frac{1}{P_r} \int_0^{\infty} P(v)f(v)dv \quad (1)$$

With :

- \bar{P} : average power produced by the wind turbine
- P_r : rated power of the wind turbine
- $P(v)$: power curve of the wind turbine
- $f(v)$: wind speed distribution

Wind speed distribution. ERA-Interim dataset, a global atmospheric reanalysis Dee et al. (2011), was used in order to estimate means and standard deviations of wind speed at a geographical grid cell level (Figure 3). In order to have a wind profile as close as possible from the wind profile at hub height, estimates of wind speed at 71 meters and 125 meters were used. The arithmetic mean was used to estimate wind speeds at 100 meters.

Wind speed data are well fitted with a Weibull distribution with probability function f :

$$f(v) = \frac{k}{c} \left(\frac{v}{c}\right)^{k-1} \exp\left[-\left(\frac{v}{c}\right)^k\right] \quad (2)$$

Shape parameter k and scale parameter c are estimated from mean wind speed \bar{u} with standard deviation σ using the empirical method of Justus Justus et al. (1978) :

$$k = \left(\frac{\sigma}{\bar{u}}\right)^{-1.086}$$

$$c = \frac{\bar{u}}{\Gamma(1 + 1/k)}$$

Wind turbine power curve. The power output of a wind turbine is modelled as follows (Figure 4):

$$P(v) = P_r \begin{cases} 0 & v < v_c, \\ \frac{v^3 - v_c^3}{v_r^3 - v_c^3} & v_c \leq v \leq v_r, \\ 1 & v_r \leq v \leq v_f, \\ 0 & v \geq v_f. \end{cases} \quad (3)$$

With v_c , v_r and v_f being respectively the cut-in, rated and cut-out wind speeds.

With expressions (2) and (3), integral (1) is resolved in order to derive an expression for the capacity factor as a function of the local weibull parameters c and k , and the wind turbine design parameters v_c , v_r and v_f . This expression is independent from the rated power.

$$C_f = -e^{-\left(\frac{v_f}{c}\right)^k} + \frac{3c^3\Gamma\left(\frac{3}{k}\right)}{k(v_r^3 - v_c^3)} \left(\gamma\left(\left(\frac{v_r}{c}\right)^k, \frac{3}{k}\right) - \gamma\left(\left(\frac{v_c}{c}\right)^k, \frac{3}{k}\right) \right) \quad (4)$$

With Γ and γ being respectively the gamma and incomplete gamma functions.

$$\Gamma(x) = \int_0^\infty t^{x-1} e^{-t} dt$$

$$\gamma(u, x) = \frac{1}{\Gamma(x)} \int_0^u t^{x-1} e^{-t} dt$$

Wind turbine specifications. The cut-in speed v_c is usually around 3-4 m/s, because at lower wind speeds there is insufficient torque exerted on the blades to make them rotate. The cut-out speed v_f is usually 25 m/s in order to avoid damage, and the rated speed v_r has a range of 11-17 m/s, depending on local wind conditions.

The power that is extracted from the wind by a turbine is given by:

$$P = C_p \frac{1}{2} \rho A v^3$$

With ρ the air density, A the rotor swept area, and C_p the performance coefficient. The maximum theoretical value of the performance coefficient is 59.26 % according to Betz law. With technological progress aerodynamic and mechanical losses are reduced. Modern large wind turbines achieve peak values for C_p in the range of 45 to 50 %. The relationship between rated power, rotor diameter, and rated wind speed for modern turbines can therefore be better expressed as:

$$P_r = C_{p,max} \frac{1}{2} \rho \frac{\pi D^2}{4} v_r^3 \quad (5)$$

For low wind speed sites, a lower rated wind speed allows for a greater capacity factor. Therefore, compared to wind turbines for high wind speed sites either the rated power is lower for the same rotor diameter, or the rotor diameter is larger for the same rated power.

3.2.2. Array placement efficiency

The theoretical capacity factor calculated in section 3.2.1 is valid for an isolated wind turbine or small wind farms. However turbines are placed increasingly into large wind farms with hundreds of turbines. When a wind turbine extracts energy from the wind, there is a wake downstream with reduced wind speed. Because wind power is proportional to the cube of wind speed, in order to reduce power losses there should be enough space between wind turbines to allow for wind speed recovery via horizontal or vertical replenishment of kinetic energy. In large turbine arrays horizontal transport

of kinetic energy can be neglected and the amount of energy that can be extracted is limited by the vertical replenishment of kinetic energy.

Various studies show that these interferences increase quite rapidly if the wind turbines are less than 10 rotor diameters (RD) apart (Meyers and Meneveau (2011)). Turbine wake interference has been widely studied, but data is so far limited on the effect for very large turbine arrays. In order to take this effect into account, a global average array efficiency inclusive of wake effects was calculated and applied to each wind farm output, based on the ratio between the output of a turbine in the wind farm to the output of the same turbine alone without any interference. It has been shown that the critical parameter constraining array efficiency is a spacing parameter λ that is the ratio of the rotor swept area to the land surface area occupied by a wind turbine in the wind farm (Templin (1974); Crafoord (1975); Stevens et al. (2016); Stevens and Meneveau (2017) and Figure 5).

We use array efficiencies for different λ and array sizes from Gustavson (1979), as per Table 3, that we fitted to a negative exponential of type $ae^{-b\lambda}$, via non linear regression with a least squares approach (Figure 6). These results are coherent with recent numerical studies which show that optimal turbine spacing in large wind farms may be considerably higher (~ 15 RD) than the 7 to 10 RD used in current configurations Meyers and Meneveau (2011).

In most studies on global wind power, the use of constant array efficiencies plausibly leads to an overestimation of the power produced. For example in EEA (2009) the array efficiency used is 90 % for offshore locations and 92.5 % for onshore locations. The assumptions on installed capacity densities in

this study ($10 \text{ MW}/\text{km}^2$ onshore and $8 \text{ MW}/1.25 \text{ km}^2$ offshore) and rotor diameters (80 m onshore and 120 m offshore) correspond to turbine spacings of 5.6 RD onshore and 9.3 RD offshore. Spacing at these RD's in large wind farms, however, does not allow for array efficiencies as high as 90%, according to Gustavson (1979). In Hoogwijk (2004); Bosch et al. (2017); Eurek et al. (2017), the authors also assume a constant array efficiency of 90 % with a turbine spacing of 5 to 7 RD, which is not consistent with the values for large arrays from Table 3.

The array effect shows that for a given area, there is a trade-off between very dense wind farms where wind turbines have low yields, and sparse wind farms where the output of each turbine is maximized.

3.2.3. Availability factor and transmission losses

Transmission losses are neglected as these occur after wind power generation. An availability factor, also referred to as production loss factor, is taken into account at 97% for onshore areas, and 95 % for offshore areas, in order to take into account the loss of capturing the wind when it blows due to sudden and periodic maintenance of turbines. These values are a conservative estimate based on recent industry reported values estimated by monitoring tens of thousands of onshore and hundreds of offshore turbines Belton (2016); The Crown Estate (2016).

3.3. Life Cycle Energy Inputs

Several existing studies calculate the EROI or a cumulative energy demand (CED) figure for wind power using life cycle approaches Lenzen and Munksgaard (2002); Crawford (2009); Martinez et al. (2009); Tremeac and

Meunier (2009). Results for net energy assessment studies can yield a wide range due to different boundary assumptions, age of manufacturing input data, and key technology assumptions Koppelaar (2017). Previously studied life-cycle stages for wind power include: the manufacturing of components, transport, installation, operation and maintenance, grid connection, and decommissioning. We expand upon these results by taking a complete cradle-to-grave boundary approach for onshore and offshore wind (fixed monopile and floating ballast), encompassing nine stages from raw materials to final decommissioning, inclusive of embodied energy from raw materials extraction and processing. Data values are presented for 1 GW of onshore and offshore wind power capacity in this section. All electricity values, except for operational parasitic load, were converted into primary grid inputs so as to obtain a primary energy equivalent EROI value Raugei (2016). The electricity to primary fuel conversion was carried out with a multiplying factor of 2.24 calculated from the 2015 global electricity mix BP (2016).

In the next two subsections first a fixed value for the energy embodied in a typical wind farm of 1 GW is estimated, for onshore, offshore fixed monopile and offshore floating. Then the increase in energy inputs with distance to coast (for all types of wind farms) and water depth (for fixed monopiles) are taken into account.

3.3.1. Life cycle data for 1 GW of wind power

The main components of a wind farm are wind tower generators, internal cables and a transformer station, plus external transmission cables for offshore wind to connect to the onshore grid. A wind tower generator is composed of a tower, nacelle, rotor, and foundation, which are individually built

and then combined on-site. The nine life-cycle stages included in this study are i) raw materials extraction and conversion to an intermediary material (such as aluminium or steel slabs or rolls), ii) transport to the factory, iii) manufacturing of the wind generator and other components, iv) transport to the installation site, v) installation, vi) operation, vii) maintenance, viii) decommissioning, and ix) decommissioning transport. Tables 4 , 5, 6, and 7 summarize the components and energy inputs associated with each stage in the life cycle for onshore and offshore wind power. Energy intensities used for materials extraction and transport calculations are given in Table 8.

The example case yields a total life cycle primary energy input for a 1 GW onshore, fixed offshore (15 m depth), and floating offshore wind farm of 20.2, 25.9, and 30.5 PJ, respectively. If for the onshore wind farm a lifetime of 25 years and a capacity factor of 22% is assumed this results in 179.5 PJ of electricity output and a life cycle EROI of 8.9. If for the fixed and floating offshore wind farm the same lifetime is assumed with a capacity factor of 39% this results in 309.6 PJ electricity output and a life cycle EROI of 12, and 10.4, respectively.

Energy inputs for wind energy are dominated by extraction and processing of minerals (about 25-30% of inputs), the manufacturing of the wind turbine and grid infrastructure (about 35-40% of inputs), and the operational parasitic load (about 7-8% for 10 MW offshore and 30% for 3 MW onshore turbine parks). For offshore wind, installation (about 7-15% of inputs) and maintenance costs (about 8-10% of inputs) are significant, varying with distance. The most critical variable factor for offshore is the foundation (typically steel monopiles), which increases in weight with water depth and

turbine size, raising raw material and installation energy costs, although this is compensated for by higher offshore load factors. Offshore grid connection costs are also substantial at 0.5 PJ in embodied and installation energy for every 100 km of 132 kV cable.

3.3.2. Influence of distance to coast

Final transport distance for installation and maintenance was variably incorporated for both onshore and offshore wind farms. The mean distance to the nearest coast for each 0.75° grid cell for wind generator installation was taken from NASA's Ocean Biology Processing Group dataset NASA (2009). The distance was multiplied by the fuel intensity values in Table 8. An additional fixed distance for installation of 600 km for truck and 10,000 km for ship transport was incorporated from factory to port Garrett and Ronde (2013). Raw materials extraction plus processing and ship transport distances were incorporated using a static value as per Table 6. The nearest coast distance factor was also applied to the transmission cables from substation to shore for offshore wind, based on values in E.ON (2012b,a).

3.3.3. Influence of water depth

The impact of water depth on offshore wind was incorporated using a scale factor given in Table 9 based on the values in Energinet.dk (2015); Kielkiewicz et al. (2015). The factor was applied to monopile steel and ballast concrete requirements per wind generator. Mean water depth of every grid cell was taken from 1 arc-minute global relief model of Earth's surface of NOAA Amante and Eakins (2009). Scaling was limited to water depth up to 40 meters, with nearly all fixed foundation projects built up to this depth

EWEA (2013). At greater depths floating substructures will be employed in the future, potentially up to a kilometer of water depth. Several prototypes are in operation, and 200 MW of demonstration projects are underway in Scotland and France Snieckus (2017). The closest to operation is the Statoil funded HyWind project, based on a ballast design, for which specific steel and concrete values are available Statoil (2015). On the basis of this project for water depths greater than 40 meters concrete and steel values of 375,000 and 275,000 tonnes for 1000 MW of wind were taken into consideration, replacing the monopile offshore foundation values in Tables 4, 5, 6, and 7. All other calculations at depths greater than 40 meters were similar to non-floating offshore wind.

3.4. Installed Capacity Optimization

By combining results from the previous sections, the energy outputs and associated EROI for a given installed capacity in each grid cell can be estimated. Previous studies on global wind power potentials take the assumption of a constant installed capacity density, varying in general from 2 to 10 MW/km², with a constant array efficiency independent from turbine spacing and array size. But given wake effects within a wind farm (Section 3.2.2), there is an optimal installed capacity in order to maximize energy output. In this study we propose a new approach with a varying installed capacity density, in order to maximize the net energy produced over a wind farm's lifetime in every grid cell.

Given Eq. (5), and with the farm configuration as in Figure 5, the installed capacity density is expressed as a function of the rated wind speed v_r

and the spacing parameter n :

$$CD(v_r, n) = \frac{P_r}{(nD)^2} = \frac{C_p 1/2 \rho \pi / 4 v_r^3}{n^2} [\text{MW}/\text{km}^2] \quad (6)$$

For example, a 2 MW turbine with a rated speed of 11 m/s has a rotor diameter of 80 m, and occupies 0.31 km² with $n=7$, while a 10 MW turbine with the same rated speed has a rotor diameter of 176 m and therefore occupies the same land area as five 2 MW wind turbines. Knowing that the capacity factor depends on v_r only and that the array efficiency depends on n only, not only the installed capacity but also the energy produced per unit of area does not vary with turbine size, with the hypothesis described in Section 3.2.

Under the considerations above, an optimization problem can be solved for each cell: find for each cell i the optimal installed capacity, i.e. the optimal rated speed $v_{r,i}$ [m/s] and spacing parameter n_i in order to maximize net energy produced.

$$\text{Net Energy Produced} = \text{Energy Produced} - \text{Energy Inputs} \quad (7)$$

With:

$$\text{Energy Produced}_i = C_{f,i} \eta_i \text{MW}_i \text{Life Time} \quad (8)$$

- $\text{MW}_i = CD(v_{r,i}, n_i) * \text{Suitable Area}_i$: the installed capacity in cell i , i.e. the installed capacity density from Eq. (6) over the suitable area of cell i .
- $C_{f,i} = C_f(v_{r,i})$: the capacity factor of cell i for the rated wind speed $v_{r,i}$, as calculated in Section 3.2.1.

- $\eta_i = \eta(n_i)$: the array efficiency for the spacing parameter n_i over the suitable area of cell i , as calculated in Section 3.2.2.

The energy inputs for a wind farm of size MW_i on cell i , are calculated inclusive of water depth variability as per Section 3.3.

The solution must be such that the EROI in cell i is greater than a given threshold:

$$\text{EROI}_i \geq \text{EROI}_{min} \quad (9)$$

EROI_i is calculated as the net energy produced:

$$\text{EROI}_i = \frac{\text{Energy Produced}}{\text{Energy Inputs}} = \frac{C_{f,i} \eta_i \text{MW}_i \text{Life Time}}{\text{Energy Inputs}(\text{MW}_i)}$$

In some cells it may not be possible to reach EROI_{min} because the wind speeds are too low.

The reason for including a minimum EROI is that at a particular threshold the scaling of the energy sector to meet self-consumption becomes potentially too large. Energy self-consumption to build, install, and operate the turbines becomes too large for extraction to be feasible from an economic point of view of maintaining growth and living standards. When summing mean power produced, or annual energy production in each cell, an upper limit on the global wind power potential as a function of EROI_{min} is obtained.

3.5. Kinetic Energy Available

The approach presented in Section 3 so far neglects energy conservation laws. Implicitly an assumption was made that extracting a large amount of wind power has no impact on global wind generation and therefore does not alter the total production potential. The array effect, that takes into

account local wind speed reduction, is considered independent from total capacity, therefore large-scale atmospheric processes that constrain global winds are neglected.

Based on literature results presented in Section 2.2, we propose a simplified approach to take into account the limited rate of kinetic energy available. We start from the estimate of 292 TW of the kinetic energy dissipated in the atmospheric boundary layer over the globe Hermann (2006). Since turbulent dissipation is linked to the wind speed squared, we make the assumption that this power is distributed over each cell proportionally to the mean wind speed squared :

$$\text{Kinetic Energy Generation Rate}_i \sim \frac{\bar{v}_i^2 A_i}{\sum_{j \in world} \bar{v}_j^2 A_j} 292 \text{ TW} \quad (10)$$

In order to take into account the estimated kinetic energy generation rates, the following constraint is added to the maximization problem described in 3.4 :

$$\text{Power Produced}_i \leq \text{Kinetic Energy Generation Rate}_i \quad (11)$$

3.6. Net Energy Results Calculation

In each cell the rated speed and spacing parameter are computed, by maximizing the function of two variables Eq. (7) with constraints Eq. (9) and Eq. (11). The optimization procedure is repeated for different level of EROI_{min} , and the global potential is then calculated by summing the gross or net energy theoretically produced per year with those optimal parameters. For a given EROI_{min} , a function for the evolution of the EROI with annual production is obtained by classifying the sites by decreasing EROI and then by drawing the evolution of the EROI with cumulated annual production.

4. Results

4.1. Wind Farm Design Optimization

4.1.1. Capacity factors

Capacity factors calculated with Eq.(4) with a constant rated wind speed of 11 m/s are shown in Figure 7. Results are compared with capacity factors of existing onshore wind farms in Table 10. The comparison shows that the calculated capacity factors for low wind speeds (class III) are higher than the U.S. Energy Information Administration (EIA) values from 2013-2014 for most countries. These results are mainly dependent on the rated wind speed, as a higher rated wind speed would yield lower capacity factors.

4.1.2. Optimization variables ($v_{r,i}$ and n_i)

As explained in Section 3.4, the net energy that can theoretically be produced in each cell is maximized by optimizing the wind turbine design, via the rated wind speed v_r , and the wind farm configuration, via a spacing parameter n representing the spacing between two wind turbines in the wind farm in units of rotor diameter (RD). The optimal values directly give the optimal installed capacity densities, and, with results from the methodology in Section 3.2, the energy produced is computed. In order to remain within realistic turbine designs, the rated wind speed was allowed to vary from 10 to 16 m/s and the spacing parameter from 1 to 20 RD. The found results for the optimal value range was found to be between 10 and 13.65 m/s for the optimal rated speed, and from 6.8 to 20 RD for the optimal spacing parameter, corresponding to installed capacity densities varying from 0.6 to 9.26 MW/km².

The minimum value for the optimal spacing parameter increases with $EROI_{min}$, to values that are greater than current configurations but more consistent with results from wake aerodynamic studies (i.e. a spacing between each turbine varying between 12 to 20 RD) Meyers and Meneveau (2011); Stevens et al. (2016); Stevens and Meneveau (2017).

4.1.3. Kinetic energy generation rates

The global rate of kinetic energy available on suitable areas is assessed with Eq. (10). If restrictions are set to allow only onshore areas and offshore areas with water depths below 1 km, the 292 TW global total is reduced to 68 TW. In combination with the suitability factors defined in Section 3.1, the resulting available energy potential is 15.85 TW over suitable onshore areas and 8.35 TW over suitable offshore areas.

4.2. Global Optimization Results

4.2.1. Evolution of the cumulative available wind energy flux based on EROI values

The results for the available energy that can be extracted from wind power is shown in this section, based on a curve, as described in Section 3.6, with the total production potential from the optimization on the x-axis, relative to the EROI value on the y-axis. The shape of this curve gives a good idea of the repartition of the resources, i.e. if the initial slope is very steep, high EROI resources are limited. If in contrast there is a plateau at high EROI values it means that many places on earth are suitable to produce electricity from wind with only low energy input requirements relative to energy output.

In Figure 8a the results with no constraint on $EROI_{min}$ is shown. The

initial slope is quite steep, indicating that only a small part of the available wind energy flux is available with high EROI values. The potential for EROI greater than 10 equates 89 EJ/year out of a total global value of 767 EJ/year.

In the same graph (Figure 8a), the resulting function when EROI_{\min} is fixed at 8 (dotted line) is shown. The curve for $\text{EROI}_{\min}=8$ follows the unconstrained curve until an EROI of 8, where there is a plateau until the potential drops to zero, because all sites where no wind park configuration allows for an EROI above 8 are excluded. The total potential available wind energy flux at this EROI amounts to 536 EJ per year globally, compared to 312 EJ in the unconstrained case. Surprisingly, the constraint on EROI_{\min} allows to reach a significantly higher potential for the same level of EROI. This is because the EROI_{\min} constraint forces less dense farms on certain cells in order to increase the energy outputs per MW installed, and reach the EROI_{\min} imposed. In the following graph (Figure 8b) the curves for EROI_{\min} of 5 and 12 are added. Because optimal parameters depend on the EROI_{\min} required, the evolution of the EROI with annual production will be slightly different for each value of EROI_{\min} . The total global potential available wind energy flux at an EROI_{\min} of 5 and 12 are 709 EJ/year and 99 EJ/year, respectively.

4.2.2. Enveloppe of the wind potential

The results for the various evaluated EROI_{\min} levels as described above can be combined to generate an enveloppe curve of the total available wind energy flux, as shown in Figure 8c. The curve can be used to read the potential available wind energy flux for every EROI_{\min} value from 1 to 20. The results using this enveloppe curve including variation by EROI_{\min} are

given in Table 11. For example, for an $EROI_{min}$ of 5 an upper limit of 709 EJ per year is found, but it is reduced to 7 EJ/year for an $EROI_{min}$ of 15. As a comparison, global primary energy consumption was about 550 EJ in 2015 BP (2016), and is expected to be in the range of 700-830 EJ by 2040 WEC (2016); IEA (2016).

4.2.3. Onshore - offshore repartition

In Figure 9a, the available energy flux is further divided into onshore and offshore areas. Onshore potential is higher for low EROI values, with a total flux of 519 EJ/year available compared to 248 EJ/year for offshore areas. When $EROI_{min}$ exceeds 12, the offshore potential exceeds onshore potential. As shown in Figure 9b, where the offshore potential is further divided by water depth, a significant part of the potential is in deep water (> 50 m depth). The total available energy flux for water depth between 50 meters and 1000 meters water depth is 200 EJ/year versus 48 EJ/year for depths lower than 50 meters.

4.2.4. Spatial distribution of the resources

Results are shown on a world map for two values of $EROI_{min}$ to visualize the evolution of the spatial distribution of the resources. In Figure 10a optimal installed capacity densities are shown for $EROI_{min} = 5$, with a resulting mean installed capacity density of 1.98 MW/km². In Figure 10b optimal installed capacity densities are shown for $EROI_{min} = 12$ with a mean installed capacity density of 1.05 MW/km².

The same analysis was conducted for power densities based on the mean power produced per unit area. The mean value increases with $EROI_{min}$. At

a low EROI_{\min} of 5 the mean is $0.37 \text{ W}_e/\text{m}^2$ (0.3 over land and 0.54 over sea), and it increases to a mean of $0.57 \text{ W}_e/\text{m}^2$ for $\text{EROI}_{\min} = 15$. These results are coherent with results of global circulation models from Miller and Kleidon (2016).

4.2.5. Limit on wind power density

A sensitivity analysis was run to illustrate the impact of the constraint from Eq.(11). The results are compared with 3 other scenarios in Figure 11 : first by applying a factor 1.5 to the estimate from Eq. (10), then with a constant upper limit of $1 \text{ W}_e/\text{m}^2$, and third with no upper limit on the wind power density. The difference between the curves when EROI_{\min} decreases is substantial, with a total available global wind energy flux of 1988 EJ/year for the unconstrained case. However for $\text{EROI}_{\min} \geq 10$ all scenarios yield similar potentials. Indeed, for high EROI values the optimal installed capacity densities are relatively low in order to maximize the output of each turbine. With sufficiently sparse wind farms, the power densities are not exceeding the upper limit from Eq.(10), and the 4 scenarios are converging for high EROI values.

4.2.6. Installed capacity densities

The enveloppe for the wind potential is also compared with the results of the model using fixed installed capacity densities in Figure 12. This emphasizes the benefit of the optimization, since the global EJ/year potential remains constant but the curve shifts to lower EROI values when installed capacity density increases from 2 to $9 \text{ MW}/\text{km}^2$. Beyond $2 \text{ MW}/\text{km}^2$, the array effect becomes increasingly significant, as explained in Section 3.2.2.

Therefore, adding more turbines does not allow to produce more electricity per unit of area.

4.3. Regional Optimization Results

Results can also be computed for a specific area, so as to find a realistic constraint on the available wind resource per region or country that can be applied in energy modelling and to inform policy design. The first approach, as shown here first for the whole world (Section 4.3.1) and then for the European Union (EU-28) countries (Section 4.3.2), is to assess the regional potential for a given cut-off EROI_{min} . Then we do the same exercise with a minimum capacity factor requirement, for comparison purposes (Section 4.3.3).

4.3.1. Regional potentials

The about 100 EJ/year of high EROI resources ($\text{EROI} \geq 12$) are distributed as follows (Table 12 and Figure 10b):

- 20% in North America, mainly the North and East coasts of Canada (75 % of the potential), evenly distributed among onshore and offshore areas.
- 16% in Patagonia (southern Chile and Argentina), evenly distributed among onshore and offshore areas.
- 15.5% in Europe, especially in the UK (40 % of the potential), Ireland, Norway, and Iceland, and mainly offshore (77 % of the potential).
- 14% in Oceania, mainly in the Tasman sea around New Zealand (80% of the potential).

- 14% in Africa (Morocco, Western Sahara, Mauritania, Sudan, Chad, East-Ethiopia, and Somalia), onshore.
- 13% along the Russian coast line, mainly onshore (70 % of the potential).

Among the remaining 6% the highest shares are in Kazakhstan, Brazil, China, Venezuela, and Japan.

4.3.2. EU-28 countries

Results for the EU-28 countries are shown in Figure 13a, divided into onshore and offshore potential. The upper limit for the available wind energy flux in the EU-28 territories ranges from 34 EJ for $\text{EROI} \geq 5$, to 0.4 EJ for $\text{EROI} \geq 15$. Final energy consumption within the EU-28 countries in 2014 was 1 061.7 million tonnes of oil equivalent (Mtoe) Eurostat (2014), equivalent to 44.5 EJ, while wind energy production was accounting for 2 % of that consumption.

The spatial repartition of these resources is shown in Figures 14a and 14b, where the optimal installed capacity densities are shown for 2 levels of EROI_{min} . The potential for countries with high EROI resources is detailed in Table 13. The offshore potential represents 58 % of the potential with $\text{EROI} \geq 5$, and 75 % of the potential with $\text{EROI} \geq 12$. As already mentioned below, about a half of the EU-28 potential with $\text{EROI} \geq 12$ is located in the UK.

These results are compared with results from the EEA study EEA (2009). In their analysis, the installed capacity densities used were 10 MW/km² for onshore areas, and 6.4 MW/km² for offshore areas. By applying land-use

constraints and wind regime constraints, the authors estimated an economically competitive potential for 2030 of 97 EJ/year over onshore areas and 12.25 EJ/year over offshore areas (restricted to water depths below 50 m). The results based on these capacity density parameters were reproduced here as shown in Figure 13b. The high installed capacity densities as applied by EEA yield very low EROIs. Indeed in Figure 13b there is no potential with $\text{EROI} \geq 5$. For $\text{EROI} \geq 2$ the global potential is of 25 EJ/year, only one fourth of their estimated economically competitive potential of 109 EJ/year.

4.3.3. Regional potentials with minimum capacity factor requirement

The second approach to calculate regional potentials is taken from and compared with Bosch et al. (2017) for onshore wind for comparative purposes. Bosch et al. (2017) took into account only areas with a wind capacity factor $> 15\%$ in computing the onshore wind potential. In all regions we find a five times lower onshore potential, and in India, Russia and South Asia a ten times lower potential, as shown in Table 15. Key differences include an assumed fixed installed capacity density of 6.52 MW/km^2 and 90% wind farm efficiency in Bosch et al. (2017) which lead to significantly inflated potentials relative to our study where the mean installed capacity density is in that case 2 MW/km^2 and the corresponding wind farm efficiency is around 82 %.

The onshore potentials found in this study based on this approach are lower than the required outputs of onshore wind in several recent 100% renewable energy scenarios. For example, Gulagi et al. (2017) require 467-616 TWh of onshore wind output per year to reach 100% renewable electricity in India. And the analysis of Jacobson et al. (2017) utilises 3,028 TWh of onshore wind to reach 100% renewable energy including heat and transport

in India. For China Jacobson et al. (2017) requires 8,271 TWh/year versus a maximum potential of 6,195 TWh/year in our study when limiting to > 15% capacity factor areas (Section 4.3.1).

5. Discussion

The three novel contributions of this work are the inclusion of an upper limit for the wind power density (Eq.(11)), the optimization of installed capacity densities, and the evaluation of total available wind energy flux relative to the EROI of wind turbine based power generation. The model does not take into account the distance to electricity consumers, and therefore a significant portion of the available energy flux is plausibly located in remote areas.

5.1. Comparison with previous bottom-up studies

Because we use a similar approach to bottom-up studies reported in Table 1, results should be in similar order of magnitude. In these studies the available areas are restricted to areas with mean wind speed greater than class III ($v_{10m} \geq 4$ m/s, equivalent to $v_{70m} \geq 6$ m/s), based on the hypothesis that this wind speed limit corresponds to economically viable sites. In Table 14 results for onshore areas with mean wind speed greater than class III are given, with optimal parameters and installed capacity densities from Hoogwijk (2004); Honnery and Moriarty (2009); Archer and Jacobson (2005).

We conclude that only the lower estimates of studies using capacity densities of 4 MW/km² or lower (Hoogwijk (2004) and Honnery and Moriarty (2009)) are consistent with our approach for the available maximum wind energy flux. For studies with installed capacity densities above 4 MW/km²,

the literature results are an order of magnitude higher than our results. The reason is the overestimation of array efficiency in these literature studies according to our analysis (Section 3.2.2). The optimization of capacity densities for wind farms and regions is thus of key importance to ensure higher EROI extraction of the available wind resources.

The comparison with the key 100% renewable energy scenario studies of Jacobson et al. (2017) for 139 regions and detailed regional studies such as Gulagi et al. (2017) showed that for specific countries such as India and China the required scenario potential is higher than the realistic upper bound for onshore wind potential. Further country by country study is required to analyse what are realistic upper bounds inclusive of wind-regime and land constraints, for application in renewable energy scenario studies and to inform policy design.

6. Conclusions and Policy Implications

The study provided a new method including land constraints, wind regimes, kinetic energy limits, and EROI constraints, to analyse the global available wind energy potential. Constraints impacts were evaluated at three levels: i) only bottom-up constraints including land use, capacity factors, and array efficiency, ii) an added minimum Energy Return on Investment value ($EROI_{min}$), iii) inclusion of a top-down limitation on the kinetic energy available in the atmospheric boundary layer. The global wind energy potential at these three levels of constraints is as follows:

- Only bottom-up constraints, a global available annual wind energy flux of 1988 EJ/year, of which 1226 EJ/year from onshore and 762 EJ/year

from offshore wind.

- Bottom-up + $EROI_{min}$ constraints, a global available wind energy flux at an $EROI_{min}$ constraint of 5, 8, 10 and 12 yielded a global wind energy flux of 1568, 707, 356 , and 104 EJ/year. The underlying values broken down into onshore wind are 1011, 437, 215, and 52 EJ/year and for offshore wind are 556, 271, 141, and 52 EJ/year, respectively.
- Bottom-up + Top-down + $EROI_{min}$ constraints, a global wind available energy flux inclusive of an $EROI_{min}$ constraint of 5, 8, 10, and 12 was found as 709, 536, 322 , and 99 EJ/year, respectively. The result is composed of an onshore wind potential of 475, 342, 196, and 49 EJ/year and an offshore wind potential of 234, 194, 125, and 50 EJ/year, respectively.

The results can be further split into regional potentials as shown in Table 12, and in Table 13 for the EU-28 territories. Total EU-28 potential net of energy inputs for bottom-up + top-down constraints are 30, 26, 21, and 11 EJ/year at an $EROI_{min}$ of 5, 8, 10 and 12, respectively.

Similarly, constraints can be set to capacity factor minimum which at >15% shows for onshore wind an upper potential of 435 EJ/year, and a value of 36, 22, 1, 51, and 26 EJ/year for Canada, China, India, Russia, and the USA, respectively.

Five key implications for energy policy and wind energy investment can be drawn. First, the study confirms that scenarios assuming wind can reach a multi-digit share of global energy production are realistic. If only the best onshore and offshore wind sites with an $EROI_{min}$ of 12 are fully occupied

99 EJ/year would be captured, based on optimally designed 4 TW and 3 TW of onshore and offshore wind capacity, or around 20% of current global energy use. This would require installing 8 times current onshore and 214 times offshore capacity relative to 2016 onshore and offshore wind capacity of 0.485 and 0.014 TW. Second, the study finds that floating offshore wind is an essential policy priority to unlock the total potential, given the offshore potential of < 50 m is half the potential of 50 to 200 m depth waters. Third, power and turbine density design of large wind parks tailored to local winds is key, so as to gain the maximum energy output at lowest cost. If not taken into account it can result in local overbuilding of capacity, lowering of capacity factors, and not capturing a portion of the available energy flux. Optimal turbine spacing varies significantly per site, with a rotor diameter distance between turbines ranging from 7 to 20 (12 to 20 for $\text{EROI}_{min} \geq 10$), equivalent to capacity density of 0.6 to 9.3 MW/km² (0.6 to 3.2 MW/km² for $\text{EROI}_{min} \geq 10$). Fourth, the use of dynamic capacity and power densities for regional wind energy potential is essential, as studies taking fixed densities without taking constraints into account can lead to substantial overestimates. As an example in this study the EU-28 territories potential for onshore wind was established at 12 EJ/year, versus 97 EJ/year in EEA (2009) due to more realistic power and capacity density constraints. Five, the use of detailed upper constraints on wind energy at a regional and country level is key in building energy scenarios so as to reach energy policies outcomes that are based on realistic available resource potentials.

Further work to inform policy will be carried out in two respects. First, to carry out more precise analyses of top-down kinetic energy constraints using

global circulation models. Second, to specify country by country potentials using the combined constraints methodology inclusive of land use and planning.

Finally, a general recommendation for further study is to assess what EROI_{min} factor consists of a suitable cut-off factor from an economic perspective, in context of an electricity system with double-digit wind energy shares, since many countries only have a < 10 EROI wind resource available.

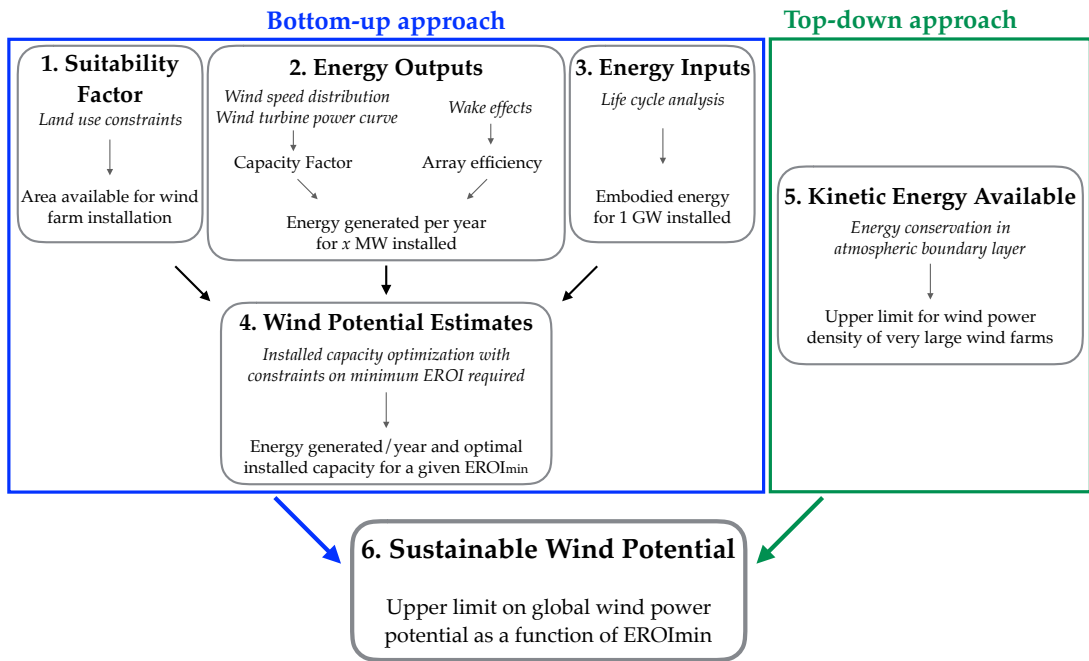


Figure 1: Methodology used in this study to estimate the evolution of the EROI of wind energy with cumulated annual production.

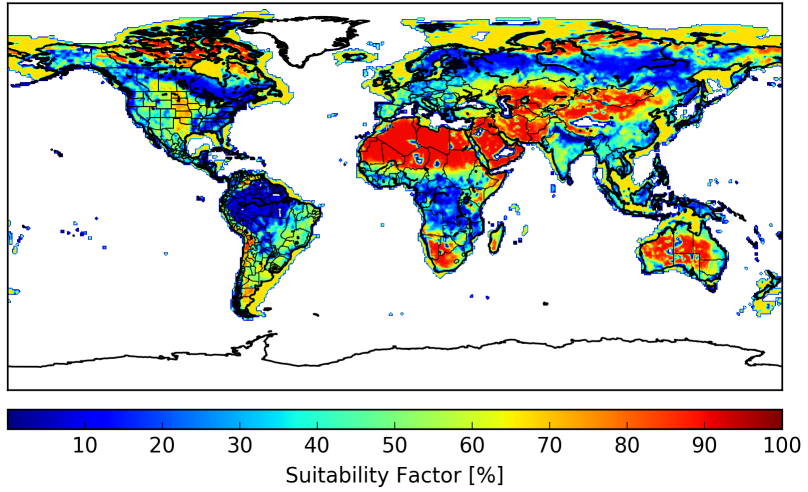


Figure 2: Map of the suitability factor, i.e. the proportion of each cell that is considered as suitable for wind farm installation in the model.

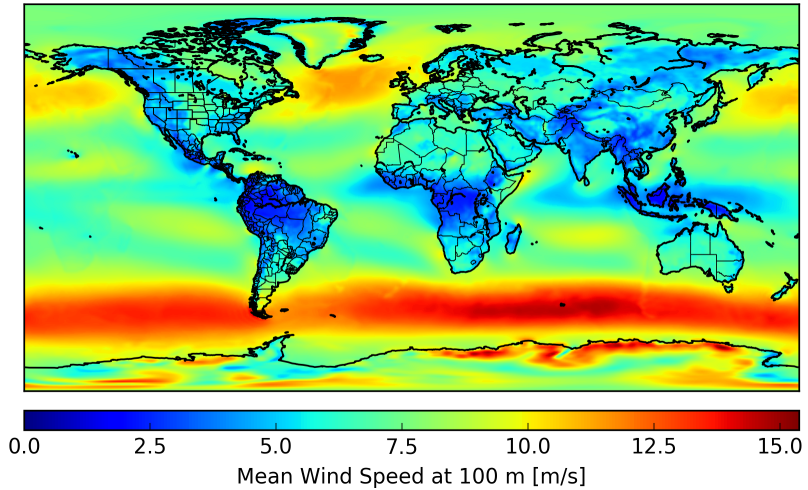


Figure 3: Mean wind speed estimates at 100 m, calculated based on data obtained from ERA-Interim reanalysis Dee et al. (2011), every 6 hours from 01-01-2007 to 31-12-2016, at a $0.75^\circ \times 0.75^\circ$ precision.

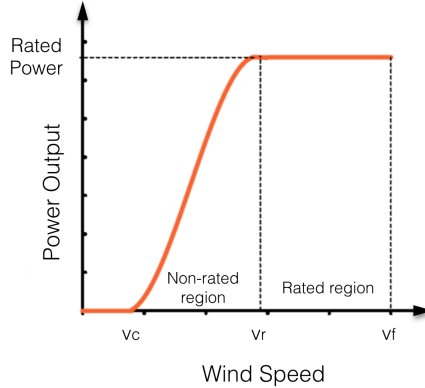


Figure 4: Typical wind turbine power curve : the turbine begins to operate at the cut-in speed v_c , then the power output increases with wind speed following a cubic curve until wind speed reaches the rated speed, where the turbine begins to operate at its rated power. The rotor is stopped when the wind speed exceeds the cut-out speed, in order to prevent damages. Typical values ranges are $v_c = 3-4\text{m/s}$, $v_r = 11-17 \text{ m/s}$ and $v_f = 25 \text{ m/s}$.

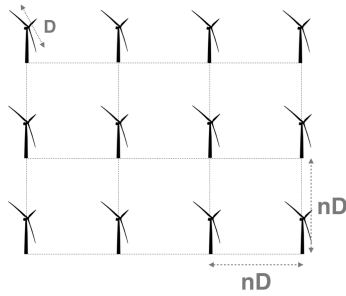


Figure 5: Wind farm configuration : we assume wind turbines are regularly placed in arrays, the spacing is expressed as a multiple n of the rotor diameter D . With such a configuration, the spacing parameter λ is a fonction of n^2 only ($\lambda = \frac{\pi D^2/4}{(nD)^2} = \frac{\pi}{4n^2}$).

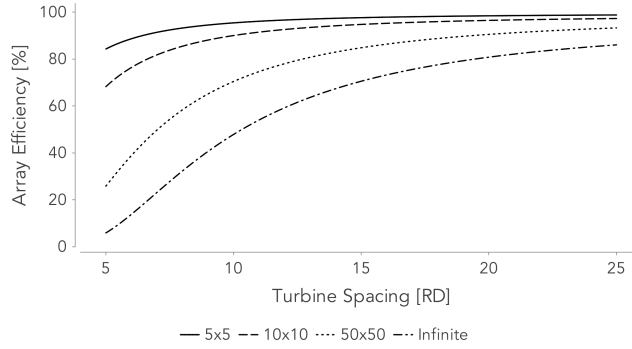


Figure 6: Array efficiency as a function of turbine spacing, for different array sizes, data from Gustavson (1979) fitted to a negative exponential : $\eta \sim ae^{-b\lambda}$.

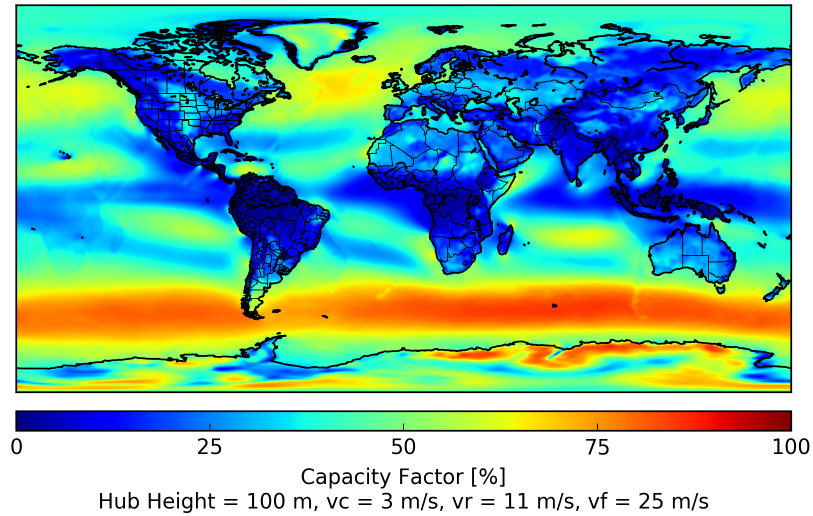
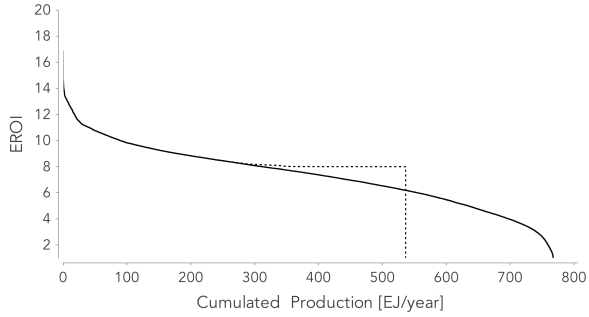
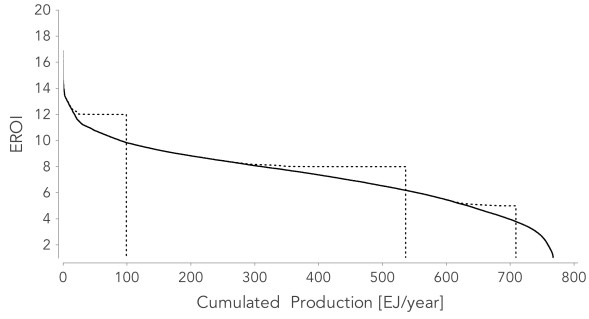


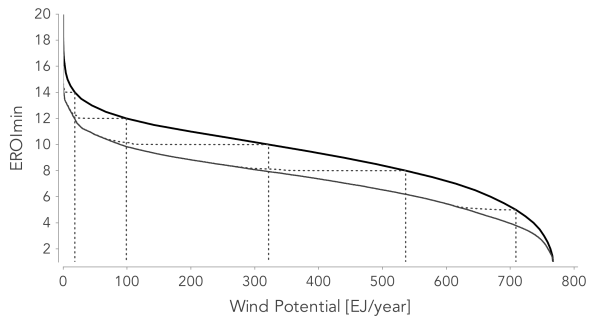
Figure 7: Map of capacity factor estimates.



(a) EROI function with no constraint on $EROI_{min}$
(plain line), and for $EROI_{min}=8$ (dotted line).

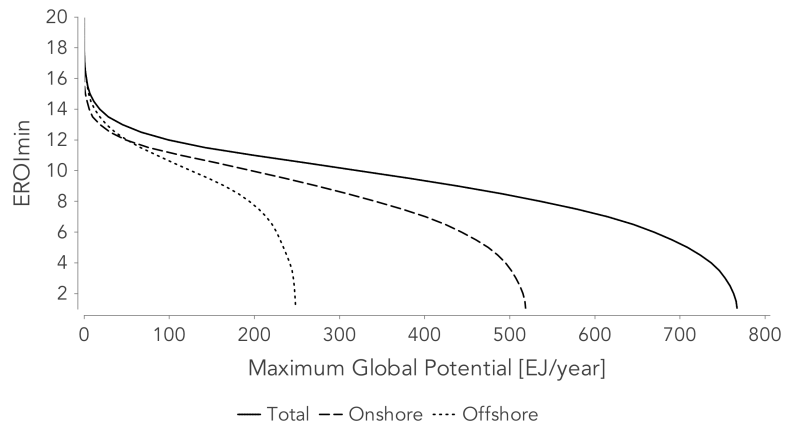


(b) EROI function with no constraint on $EROI_{min}$
(plain line), and for $EROI_{min}$ of 5, 8 and 12 (dotted
lines).

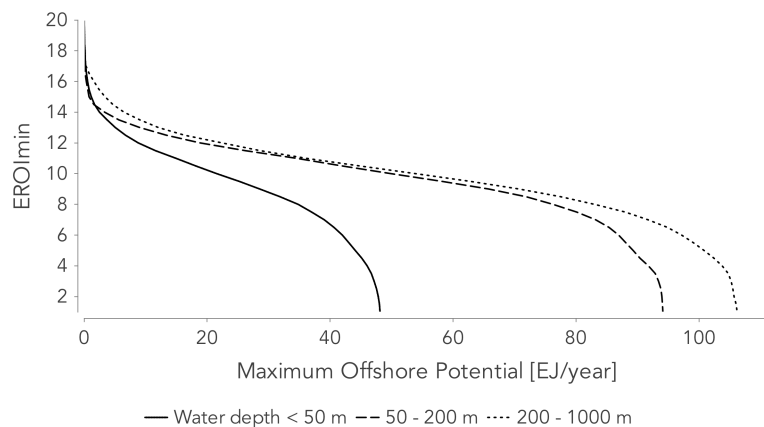


(c) Enveloppe of the wind potential as a function of
 $EROI_{min}$.

Figure 8: Construction of the enveloppe for the wind potential, i.e. the maximum potential achievable for a given $EROI_{min}$.

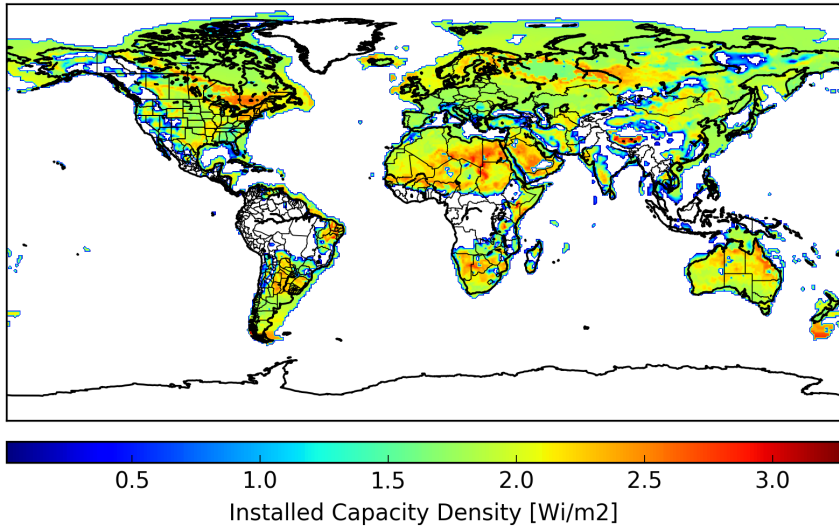


(a) Onshore - offshore repartition.

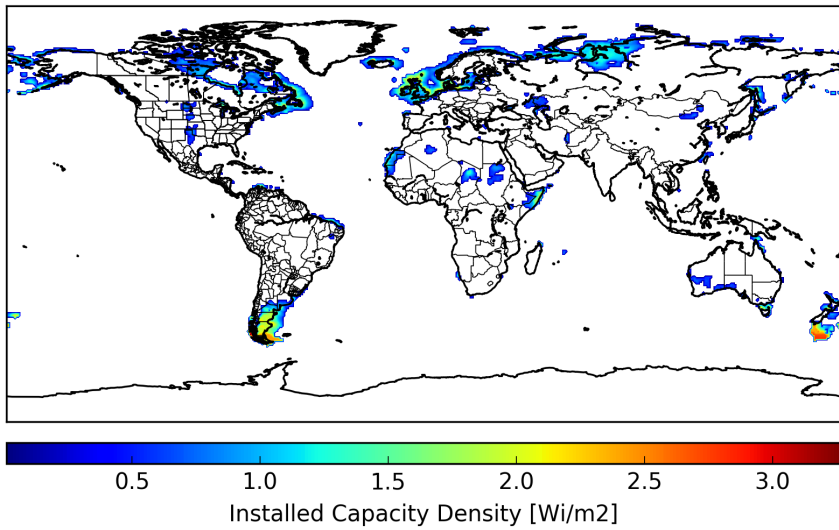


(b) Offshore repartition by water depth.

Figure 9: Repartition of the global potential between onshore and offshore areas (Figure 9a), and of the offshore potential divided by water depth (Figure 9b).



(a) $\text{EROI}_{\min}=5.$



(b) $\text{EROI}_{\min}=12.$

Figure 10: Repartition of the optimal installed capacity densities (i.e. the wind power capacity installed by unit of area) for different EROI_{\min} , results are in $\text{W}_{\text{installed}} / \text{m}^2$.

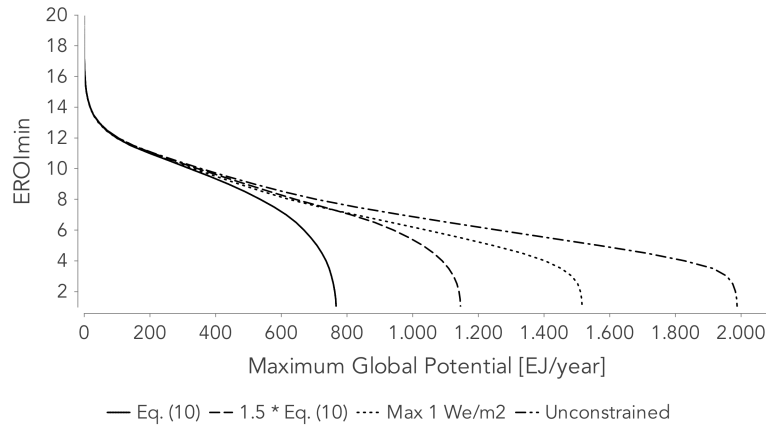


Figure 11: Impact of the constraint Eq.(11): the global gross potential [EJ/year] for different $EROI_{min}$ was optimized for 4 scenarios : first with the kinetic energy estimated from Eq.(10), then by applying a factor 1.5 to Eq.(10), third with a constant upper limit of 1 W_e / m^2 , and finally without upper limit on the wind power density.

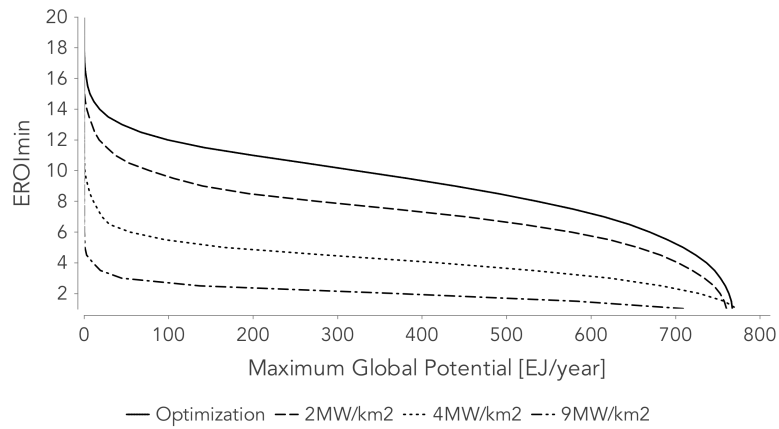
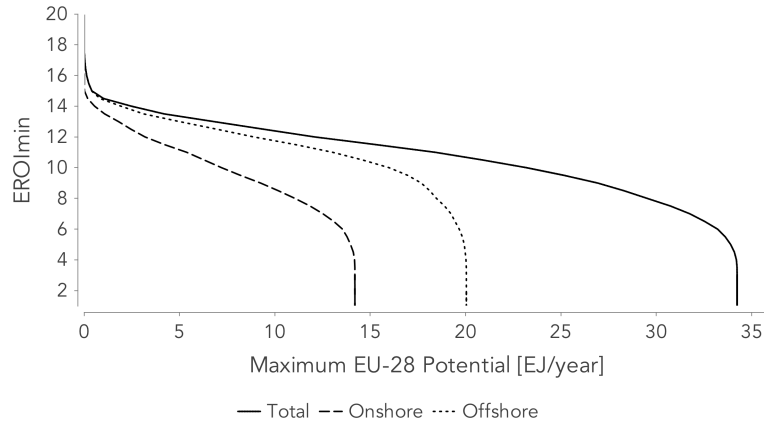
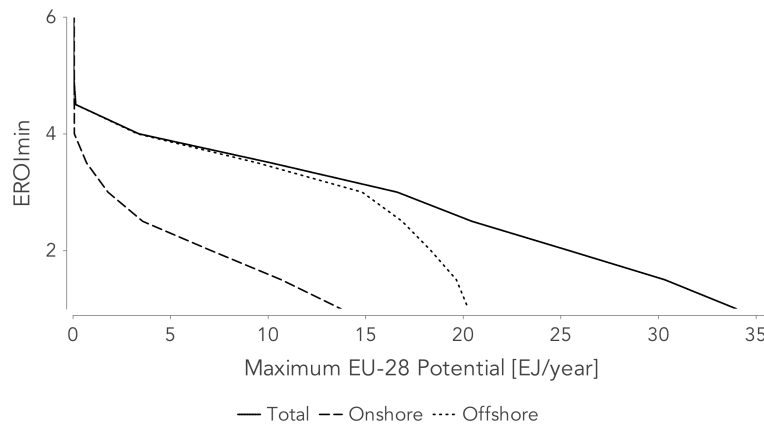


Figure 12: Enveloppe of the wind potential for different installed capacity densities. The optimization results are compared with results with fixed installed capacity densities.

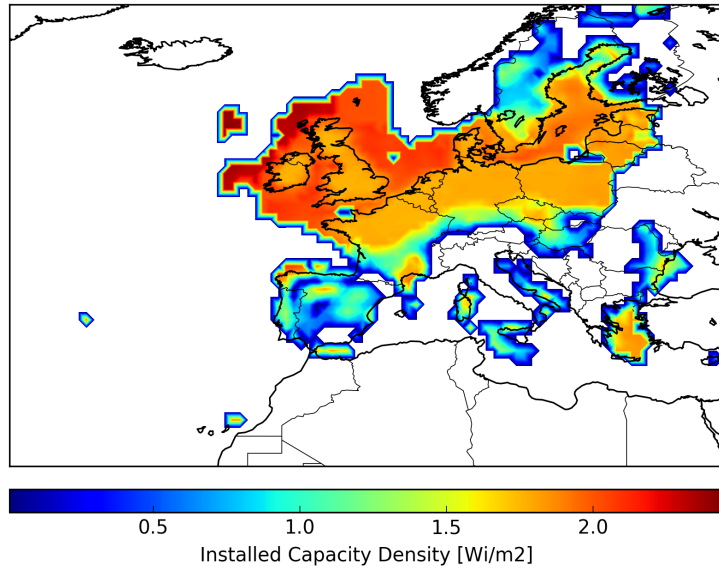


(a) EU-28's potential with the optimal installed capacity densities.

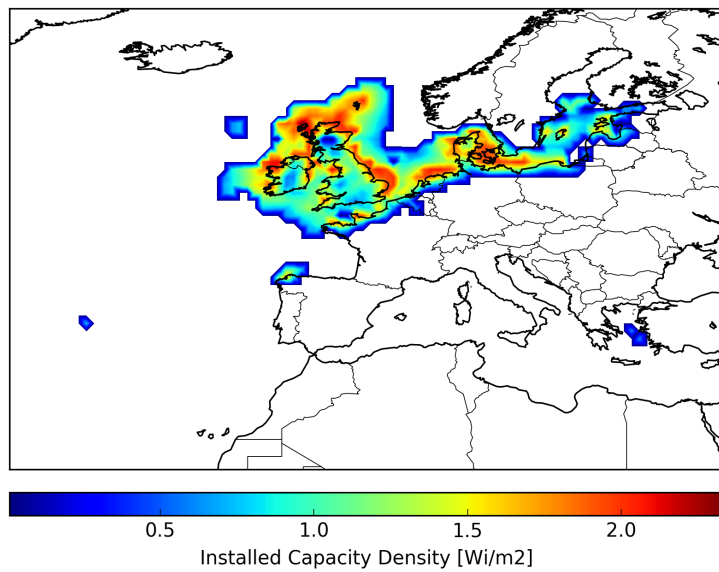


(b) EU-28's potential with installed capacity densities from EEA (2009).

Figure 13: Enveloppe of the EU-28's wind potential as a function of $EROI_{min}$, with the optimal installed capacity densities (Figure 13a) and with the fixed installed capacity densities from the EEA report (Figure 13b).



(a) $EROI_{min}=8$.



(b) $EROI_{min}=12$.

Figure 14: Repartition of the optimal installed capacity densities in EU-28 countries (i.e. the wind power capacity installed by unit of area) for different $EROI_{min}$, in $W_{\text{installed}} / m^2$.

Authors	Estimated Potential [EJ/year]	Scope	Wind regime constraints	Land use constraints?	Installed Capacity Density [MW/km ²]
Hoogwijk (2004)	346	Onshore	$\bar{v}_{80m} \geq 6.9 \text{ m/s}$	Yes	4
Archer and Jacobson (2005)	2,256	World	$\bar{v}_{80m} \geq 6.9 \text{ m/s}$	No	9
Honnery and Moriarty (2009)	229	Onshore	$\bar{v}_{70m} \geq 6 \text{ m/s}$	Yes	2
EEA (2009)	153	Europe	$\bar{v}_{10m} \geq 4 \text{ m/s}$	Yes	Onshore : 10 Offshore : 6.4
Lu et al. (2009)	3,024	World	$C_f \geq 20\%$	Yes	Onshore : 9 Offshore : 5.85
Miller et al. (2011)	570-2,150	World	Top-down	No	-
de Castro et al. (2011)	32	World	Top-down	Yes	-
GEA (2012)	250-1,200	World	$\bar{v}_{80m} \geq 6.9 \text{ m/s}$	Yes	-
Bosch et al. (2017)	2,112	Onshore	$C_f \geq 15\%$	Yes	6.52
Eurek et al. (2017)	2,720	World	$C_f \geq 18\%$	Yes	5

Table 1: Global wind power potential estimates.

	Land Cover	Land use factor [%]	Area [10⁶ km²]
Onshore	Sparse vegetation, grassland, barren areas	90	42.46
	Forests	10	36.65
	Croplands	70	7.31
	Shrubland	50	8.5
	Mosaic vegetation - croplands	60	17.29
	Mosaic grassland - forest or shrubland	50	8.94
	Urban Areas	0	0.28
	Excluded areas, i.e. Antarctica, Greenland, remote, protected	0	20.49
Total			149.46
Suitable			58.07
Offshore, exclusive economic zones	Distance to shore < 5 nmi	10	5.47
	Distance to shore 5 - 20 nmi	33	16.36
	Distance to shore > 20 nmi	67	127.28
	Water depth > 1000 m	0	109.72
	Protected Area	0	4.19
	Total		149.11
	Suitable		15.35

Table 2: Repartition of the available areas into land use categories, and for each category the land use factor, consistent with values from Hoogwijk (2004); Honnery and Moriarty (2009); Bosch et al. (2017); Eurek et al. (2017).

		$\lambda = \frac{A_{rotor}}{A_{turbine}} = \frac{\pi}{4n^2}$			
		0.03	0.01	0.003	0.001
		(5D)	(9D)	(16D)	(28D)
Array Size	5 x 5	85	94	98	99
	10 x 10	70	86	96	98
	50 x 50	29	62	87	95
	Infinite	10	38	73	89

Table 3: Array efficiency estimates [%], for different array sizes and spacing parameters λ , from Gustavson (1979).

Embodied energy in materials for 1 GW turbine generators							
Component	Material	Weight [tonnes]		Electricity [GJ]		Diesel [GJ]	
		Onshore	Offshore	Onshore	Offshore	Onshore	Offshore
Tower	Steel	52,920	27,500	123,282	64,064	1,184,350	615,450
	Coating	420	331	18,783	14,791	9,074	7,146
Nacelle	Steel	19,993	46,502	46,576	108,331	447,451	1,040,718
	Copper	1,250	1,754	95,358	125,726	14,634	19,294
	Aluminum	770	484	96,113	19,294	17,764	60,373
	Coating	17	7	810	323	361	144
Hub and blades	Steel	6,643	13,562	15,476	31,595	148,678	303,525
	Fibre Glass	4,013	7,217	143,838	258,639	64,213	115,464
	Epoxy Resin	2,810	5,054	251,776	452,847	112,400	202,164
	Coating	21	38	1,035	1,861	462	831
Foundation	Concrete	380,000	7,813	502,208	16,173	786,600	10,326
	Steel	12,000	155,375	27,955	361,962	268,560	3,477,293

Embodied energy in materials for substation and cables							
Component	Material	Weight [tonnes]		Electricity [GJ]		Diesel [GJ]	
		Onshore	Offshore	Onshore	Offshore	Onshore	Offshore
Park cabling (183 km)	Steel	0	1502	0	3,604	0	33,633
	Copper	266	846	20,419	64,974	2,925	9,306
	Aluminium	1358	0	181,420	0	31,349	0
	Other	1471	1463	70,648	70,242	29,437	29,267
Substation	Steel	337	337	808	808	7,540	7,540
	Copper	88	88	6,758	6,758	968	968
	Other	214.5	214.5	10,296	10,296	4,290	4,290
Cables to shore (1 km)	Steel	n/a	25.3	n/a	61	n/a	567
	Copper	n/a	19.8	n/a	1,517	n/a	217
	Other	n/a	34.1	n/a	1,637	n/a	682

Table 4: Energy inputs for 1 GW of wind.

Raw data onshore: materials Crawford (2009), substation and cables Peregrine and Fernandez de la Hoz (2013); ABB Power Transmission (2000).

Raw data offshore: materials Crawford (2009); GAMESA (2015); Livaniou et al. (2015), substation & cables ABB Power Transmission (2000); Arvesen et al. (2013).

Manufacturing primary energy [GJ]		
for 1 GW turbine generators		
	Onshore	Offshore
Wind turbine	7,869,000	8,523,000
Park cabling (183 km)	52,128	66,030
Substation	16,632	16,632
Cables to shore (1 km)	583	1,282

Table 5: Energy inputs for 1 GW of wind (continued).

Raw data: onshore Pereg and Fernandez de la Hoz (2013); GAMESA (2013), offshore GAMESA (2015).

Transport								
Transport	Material	Mode	Weight [tonnes]		Distance [km]		Diesel [GJ]	
			Onshore	Offshore	Onshore	Offshore	Onshore	Offshore
Raw materials	Cement	Truck	380,000	7,813	20	20	9,500	195
	Steel	Truck	91,557	242,939	150	150	17,167	45,551
	Copper	Truck	1,330	1,754	430	430	715	943
	Aluminium	Truck	770	484	60	60	58	36
	Other	Truck	7,282	12,647	20	20	182	316
	Copper	Ship	1,330	1,754	4,200	4,200	161	212
	Aluminium	Ship	455	484	3,000	3,000	39	42
	Other	Ship	7,282	12,647	4,000	4,000	839	1,457
Factory to Site	Cement	Truck	380,000	7,813	250	250	118,750	2,442
	Steel	Truck	91,557	242,939	600	600	57,223	182,204
	Copper	Truck	1,330	1,754	600	600	416	1,316
	Aluminium	Truck	770	484	600	600	667	363
	Other	Truck	7,282	12,647	600	600	5,462	9,485
	Steel	Ship	91,557	242,939	10,000	10,000	26,368	69,966
	Copper	Ship	1,330	1,754	10,000	10,000	383	505
	Aluminium	Ship	770	484	10,000	10,000	222	139
Decommissioning	All	Truck	480,939	265,637	350	350	210,411	116,216
	All	Ship	96,188	53,127	5,000	5,000	138,510	76,503

Table 6: Energy inputs for 1 GW of wind (continued).

Raw data onshore: installation and decommissioning Ardente et al. (2008), O&M Pereg and Fernandez de la Hoz (2013); GAMESA (2013).

Raw data offshore: installation and decommissioning E.ON (2012b,a); Arvesen et al. (2013), O&M GAMESA (2015); Arvesen et al. (2013)

Other Energy Costs

		Onshore	Offshore
Installation - Primary Energy [GJ]	Wind turbine	129,660	1,709,830
	Park cabling (168 km)	13,159	33,338
	Substation	10,603	34,991
	Cabling to shore (1 km)	n/a	4,681
Operation - Electricity [GJ/GJ]		0.035	0.007
Maintenance - Diesel [GJ/GW/year]		1,656	65,587
Decommissioning - Primary Energy [GJ]		6,450	1,283,000

Table 7: Energy inputs for 1 GW of wind (end).

Raw data onshore: installation and decommissioning Ardente et al. (2008), O&M Pereg and Fernandez de la Hoz (2013); GAMESA (2013).

Raw data offshore: installation and decommissioning E.ON (2012b,a); Arvesen et al. (2013), O&M GAMESA (2015); Arvesen et al. (2013)

Material	Electricity [GJ/t]	Fuel [GJ/t]	Source of raw data for calculations
Cement	0.6	3.0	Atmaca and Yumrutas (2014a,b)
Steel	1.0	22.4	Eurofer (2015) Lamberterie (2014); Burchart-Korol (2013)
Aluminium	55.7	23.1	International Aluminium Institute (2013); Alcoa Fjardaal (2006)
Copper	32.0	11.0	Koppelaar and Koppelaar (2016)
Epoxy resin	80		Ashby (2009); AkzoNobel International (2011)
Glass Fibre	32		Ashby (2009)
Coatings	43		Ashby (2009)
Transport	Fuel [MJ/tkm]	Source	
Truck	1.25		Nylund and Erkkilä (2005); Sharpe and Muncrief (2015) Franzese (2011)
Ship	0.29		Mackay (2015)

Table 8: Energy intensity values w/o primary conversion.

Depth [m]	0-15	15-20	20-25	25-30	30-35	35-40
Multiplying Factor	1.0	1.08	1.34	1.57	1.95	2.19

Table 9: Multiplying factor for variability in offshore foundation material inputs, based on Energinet.dk (2015); Kielkiewicz et al. (2015)

Country	2014 data from EIA			Efficiency for this study	
	Installed Capacity [GW]	Production [TWh]	Wind Farms Efficiency	Class IV $\bar{v} \geq 6\text{m/s}$	Class III $\bar{v} \geq 7.5\text{m/s}$
Brazil	5.96	12.21	23.4	21.5	-
Canada	9.69	22.54	26.5	27.1	33.7
China	115	156.08	15.5	24.1	33.1
Denmark	4.89	13.08	30.5	40.1	40.1
France	9.07	17.25	21.7	26.4	35.2
Germany	39.19	57.36	16.7	26.1	34.7
India	22.47	37.16	18.9	20.6	-
Italy	8.68	15.18	20	25.9	31.7
Poland	3.84	7.68	22.9	26.2	35.5
Portugal	4.86	12.11	28.5	25.5	-
Spain	22.98	52	25.8	27	36.1
Sweden	5.1	11.23	25.2	26.5	36.2
Turkey	3.63	8.52	26.8	26.7	35.2
UK	12.99	32.02	28.1	35.8	36.9
USA	64.23	181.66	32.3	26.5	34.8

Table 10: Capacity factors of existing wind farms by country (data retrieved from U.S. Energy Information Administration EIA (2014)) compared to the theoretical capacity factors calculated in this study (Eq. 4) for different wind classes, with a constant array placement efficiency of 90 % and availability factor of 97 %. Results are based on wind speed distribution at 100 m, and for wind turbine design parameters $v_c = 3\text{ m/s}$, $v_r = 11\text{ m/s}$ and $v_f = 25\text{ m/s}$. Usually wind farms are put on sites of class III and lower in order to be cost effective.

$EROI_{min}$	Global Potential				Area [10^6 km^2]	Onshore Potential		Offshore Potential	
	Gross Energy [EJ/year]	Net Energy [EJ/year]	Installed Capacity [TW]	Gross Energy [EJ/year]		Installed Capacity [TW]	Gross Energy [EJ/year]	Installed Capacity [TW]	
∞	2	763	645	143	70	516	115	247	28
	5	709	612	114	60	475	90	234	24
	8	536	475	66	45	342	49	194	17
	10	322	291	31	29	196	22	125	10
	12	99	91	7	8	49	4	50	3
	15	6.89	6.43	0.38	0.39	1.51	0.09	5.38	0.29

Table 11: Upper limit of the global wind potential for different values of $EROI_{min}$, expressed in gross annual production and net annual production (i.e. gross annual production - energy inputs). The potential is further divided in onshore and offshore potential.

Region/Country	Potential [EJ/year]		
	$\text{EROI} \geq 12$		
	Total	Onshore	Offshore
North America	19.75	10.25	9.49
<i>Canada</i>	<i>15.07</i>	<i>7.93</i>	<i>7.15</i>
Argentina and Chile	15.92	8.65	7.27
Europe	15.53	3.35	12.18
<i>United Kingdom</i>	<i>5.65</i>	<i>1.63</i>	<i>4.02</i>
<i>Norway</i>	<i>2.24</i>	<i>0.09</i>	<i>2.16</i>
<i>Ireland</i>	<i>2.11</i>	<i>0.32</i>	<i>1.78</i>
<i>Iceland</i>	<i>1.44</i>	<i>0.1</i>	<i>1.34</i>
Oceania	14.32	1.8	12.53
<i>New Zealand</i>	<i>11.63</i>	<i>0.3</i>	<i>11.33</i>
<i>Australia</i>	<i>2.6</i>	<i>1.5</i>	<i>1.11</i>
Africa	14.28	13.07	1.21
<i>Somalia</i>	<i>3.77</i>	<i>3.53</i>	<i>0.23</i>
<i>Sudan</i>	<i>2.65</i>	<i>2.65</i>	<i>0</i>
<i>Western Sahara</i>	<i>2.14</i>	<i>1.63</i>	<i>0.5</i>
<i>Chad</i>	<i>2.12</i>	<i>2.12</i>	<i>0</i>
Russia	13.07	9.12	3.95
Kazakhstan	0.84	0.84	0
Brazil	0.82	0.38	0.44
China	0.77	0.71	0.05
Venezuela	0.22	0.07	0.16
Japan	0.19	0.05	0.14
Rest of the World	3.3	0.58	2.72
Total	99	49	50

Table 12: World regions/countries with high EROI resources ($\text{EROI} \geq 12$), classified by decreasing potential.

Country	Potential [PJ/year]			Potential [PJ/year]		
	EROI ≥ 5			EROI ≥ 12		
	Total	Onshore	Offshore	Total	Onshore	Offshore
United Kingdom	8,999	2,090	6,909	5,653	1,628	4,025
Ireland	3,530	466	3,064	2,107	324	1,783
Denmark	1,411	259	1,151	906	234	672
France	3,499	2,257	1,242	669	322	347
Netherlands	949	117	831	660	69	592
Germany	1,640	1,191	449	507	212	295
Sweden	1,684	844	840	423	94	330
Poland	1,411	1,219	192	255	120	135
Latvia	598	215	383	204	50	154
Estonia	382	89	293	168	19	149
Spain	2,406	1,604	801	136	27	109
Finland	1,127	415	712	84	7	77
Belgium	195	185	10	65	58	8
Lithuania	345	254	90	23	-	23
Greece	664	111	553	21	-	21
Portugal	185	97	88	5	-	5
Italy	1508	577	931	3	3	-
Rest of EU-28	2,598	1,781	816	-	-	-
Total	33,131	13,771	19,355	11,889	3,167	8,725

Table 13: EU-28 countries with high EROI resources, classified by decreasing EROI ≥ 12 potential.

EROI_{min}	Optimal Parameters	2 MW/km ²	4 MW/km ²	9 MW/km ²
2	735	321	515	667
5	689	321	515	377
8	355	287	226	10
10	203	78	35	0
12	52	12	3	0
15	2	0	0	0

Table 14: Onshore global potential [EJ/year], restricted to areas with mean wind speed at $70 \text{ m} \geq 6 \text{ m/s}$ and without the constraint on the limited rate of kinetic energy (Eq. 11). Results with the optimal parameters are compared with constant installed capacity densities used in the literature (Table 1). Results found here are closed to results from Hoogwijk (2004); Honnery and Moriarty (2009) and the lower estimates of GEA (2012), but only up to $\text{EROI}_{min} \geq 8$. For higher EROI, the potential is significantly reduced.

Region	Suitable Area [km ²]		Technical potential $C_f \geq 15\% [\text{TWh/y}]$	
	This Study	Bosch et al. (2017)	This Study	Bosch et al. (2017)
Canada	2,896,431	2,820,408	9,971	37,760
China	2,336,744	2,004,487	6,225	25,555
European Union	1,163,162	1,231,712	3,656	14,828
India	160,914	161,933	353	3,037
Latin America	2,164,392	2,076,996	7,503	29,546
Middle East	3,300,730	3,850,136	8,812	51,006
Oceania	4,340,244	4,318,259	13,641	55,597
Rest of Africa	10,824,219	9,581,313	34,322	142,590
Russia	4,567,391	9,536,004	14,251	126,492
South Asia (except India)	252,750	223,469	684	5,653
South East Asia	109,687	964,280	263	13,864
East Asia (except China)	793,041		2,178	
USA	2,276,426	1,557,990	7,248	17,061
Total	38,863,592	41,747,248	120,858	586,750

Table 15: Regional potentials for onshore areas with capacity factor $\geq 15\%$, compared with Bosch et al. (2017)

References

- ABB Power Transmission, 2000. Environmental Product Declaration - Power transformer TrafoStar 500 MVA. Tech. rep., ABB.
- Abbasi, S., Tabassum-Abbasi, Abbasin, T., 2016. Impact of wind-energy generation on climate : A rising spectre. *Renewable and Sustainable Energy Reviews* 59, 1591–1598.
- Adams, A., Keith, D., 2013. Are global wind power resource estimates overstated? *Environ. Res. Lett.* 8.
- AkzoNobel International, 2011. Interplus 1118 Polyester Polyurethane. Tech. rep., AkzoNobel.
- Alcoa Fjardalaal, 2006. Aluminum Plant in Reydarfjordur: Fjardabyggd. Tech. Rep. July, Alcoa Fjardalaal.
- Amante, C., Eakins, B., 2009. ETOPO1 1 Arc-Minute Global Relief Model: Procedures, Data Sources and Analysis. NOAA Technical Memorandum NESDIS NGDC-24.
- Archer, C. L., Jacobson, M. Z., 2005. Evaluation of global wind power. *Journal of Geophysical Research* 110.
- Ardente, F., Beccali, M., Cellura, M., Lo Brano, V., 2008. Energy performances and life cycle assessment of an Italian wind farm. *Renewable and Sustainable Energy Reviews* 12 (1), 200–217.

Arvesen, A., Birkeland, C., Hertwich, E. G., 2013. The importance of ships and spare parts in LCAs of offshore wind power. *Environmental Science and Technology* 47 (6), 2948–2956.

Ashby, M., 2009. Materials and the Environment: eco-informed material choice, 1st Edition. Butterworth-Heinemann.

Atmaca, A., Yumrutas, R., 2014a. Thermodynamic and exergoeconomic analysis of a cement plant: Part I - Methodology. *Energy Conversion and Management* 79, 790–798.

Atmaca, A., Yumrutas, R., 2014b. Thermodynamic and exergoeconomic analysis of a cement plant: Part II - Application. *Energy Conversion and Management* 79, 790–798.

Belton, D., 2016. Technology evolution and new market developments. In: New Zealand Wind Energy Association Conference. Last Access: June 2017.

Best, W., 1978. Limits to wind power. *Energy Conversion* 19, 71–72.

Bhandari, K., Collier, J. M., Ellingson, R. J., Apul, D., 2015. Energy pay-back time(epbt) and energy return on energy invested (eroi) of solar photovoltaic systems: A systematic review and meta-analysis. *Renewable and Sustainable Energy Reviews* 47, 133–141.

Bosch, J., Staffell, I., Hawkes, A. D., 2017. Temporally-explicit and spatially-resolved global onshore wind energy potentials. *Energy* 131, 207–217.

URL <http://dx.doi.org/10.1016/j.energy.2017.05.052>

BP, 2016. BP Statistical Review of World Energy. Tech. rep., British Petroleum.

Burchart-Korol, D., 2013. Life cycle assessment of steel production in Poland: A case study. *Journal of Cleaner Production* 54 (August), 235–243.

Capellan-Perez, I., et al., 2014. Fossil fuel depletion and socio-economic scenarios: An integrated approach. *Energy* 77, 641–666.

Cleveland, C., 2005. Net energy from the extraction of oil and gas in the united states. *Energy* 30, 769–782.

Crafoord, C., 1975. An estimate of the interaction of a limited array of windmills. Tech. rep., International Meteorological Institute, Stockholm.

Crawford, R. H., 2009. Life cycle energy and greenhouse emissions analysis of wind turbines and the effect of size on energy yield. *Renewable and Sustainable Energy Reviews* 13 (9), 2653–2660.

Dale, M., Krumdieck, S., Bodger, P., 2011. A dynamic function for energy return on investment. *Sustainability* 3, 1972–1985.

Dale, M., Krumdieck, S., Bodger, P., 2012a. Global energy modelling - a biophysical approach (gemba) part 1: An overview of biophysical economics. *Ecological Economics* 73, 152–157.

Dale, M., Krumdieck, S., Bodger, P., 2012b. Global energy modelling - a biophysical approach (gemba) part 2: Methodology. *Ecological Economics* 73, 158–167.

- de Castro, C., et al., 2011. Global wind power potential: Physical and technological limits. *Energy Policy* 39, 6677–6682.
- de Castro, C., et al., 2013. Global solar electric potential : A review of their technical and sustainable limits. *Renewable and Sustainable Energy Reviews* 28, 824–835.
- Dee, D., et al., 2011. The era-interim reanalysis: configuration and performance of the data assimilation system. *Quarterly Journal of the Royal Meteorology Society* 137, 553–597.
- EEA, 2009. Europe's onshore and offshore wind energy potential, an assessment of environmental and economic constraints. Tech. Rep. ISSN 1725-2237, European Environment Agency.
- EIA, 2014. U.S. Energy Information Association, International Energy Statistics. <http://www.eia.gov/beta/international/data/browser>, last access: March 2017.
- Energinet.dk, 2015. Technical Project Description for Offshore Wind Farms (200 MW). Tech. Rep. April, Energinet.dk.
- E.ON, 2012a. Rampion Offshore Wind Farm - Draft Environmental Statement. Tech. Rep. RSK/HE/P41318/03/04/Section 30, E.ON Climate & Renewables UK Rampion Offshore Wind Limited and RSK Environmental Limited.
- E.ON, 2012b. Rampion Offshore Wind Farm ES Section 30 Carbon Balance. Tech. rep., Environmental, RSK and E.ON Climate & Renewables UK.

ESA, UCL, 2009. GlobCover 2009 (Global Land Cover Map). http://due.esrin.esa.int/page_globcover.php, last access: March 2017.

Eurek, K., Sullivan, P., Gleason, M., Hettinger, D., Heimiller, D., Lopez, A., 2017. An improved global wind resource estimate for integrated assessment models. *Energy Econ.* 64, 552–567.
URL <http://dx.doi.org/10.1016/j.eneco.2016.11.015>

Eurofer, 2015. Welcome to EUROFER, the European Steel Association.
<http://www.eurofer.org/Aboutus/EuroferPortrait.fhtml>.

Eurostat, 2014. <http://ec.europa.eu/eurostat>, last access: May 2017.

EWEA, 2013. Deep water: the next step for offshore wind energy. Tech. rep., European Wind Energy Association.

Franzese, O., 2011. Effect of Weight and Roadway Grade on the Fuel Economy of Class-8 Freight Trucks. Tech. Rep. October, Oak Ridge National Laboratory, Oak Ridge, Tennessee.

GAMESA, 2013. Environmental Product Declaration European G114-2.0MW On-shore Wind Farm. Tech. rep., GAMESA.

GAMESA, 2015. Environmental Product Declaration GAMESA G132 - 5.0 MW onshore wind farm. Tech. rep., GAMESA.

Garrett, P., Ronde, K., 2013. Life Cycle Assessment of Electricity Production from an onshore V90-2.6 MW Wind Plant. Tech. rep., Vestas.

- GEA, 2012. Global Energy Assessment - Toward a Sustainable Future. Cambridge University Press, Cambridge, UK and New York, NY, USA and the International Institute for Applied Systems Analysis, Laxenburg, Austria.
- Gulagi, A., Choudhary, P., Bogdanov, D., Beyer, C., 2017. Electricity system based on 100% renewable energy for India and SAARC. *PLoS One* 12.
URL <https://doi.org/10.1371/journal.pone.0180611>
- Gustavson, M., 1979. Limits to wind power utilisation. *Science* 204 (4388).
- Hall, C. A., Balogh, S., Murphy, D., 2009. What is the minimum eroi that a sustainable society must have ? *Energies* 2, 25–47.
- Hall, C. A., Day, J. W., 2009. Revisiting the limits to growth after the peak oil. *American Scientist* 97 (3), 230–27.
- Hall, C. A., Lambert, J., Balogh, S., 2014. Eroi of different fuels and the implications for society. *Energy Policy* 64, 141–152.
- Hermann, W., 2006. Quantifying global exergy resources. *Energy* 31, 1685–1702.
- Honnery, D., Moriarty, P., 2009. Estimating global hydrogen production from wind. *International Journal of Hydrogen Energy* 34, 727–736.
- Hoogwijk, M., 2004. On the global and regional potential of renewable energy sources. Ph.D. thesis, Universiteit Utrecht, Faculteit Scheikunde.
- IEA, 2016. World Energy Outlook. Tech. rep., International Energy Agency.

International Aluminium Institute, 2013. Global Life Cycle Inventory Data for the Primary Aluminium Industry - 2010 Data. Tech. Rep. August, International Aluminium Institute.

IRENA, 2016. REmap: Roadmap for a Renewable Energy Future. Tech. rep., The International Renewable Energy Agency (IRENA).

IRENA, 2017. Renewable Energy Auctions : Analysing 2016. Tech. rep., IRENA, Abu Dhabi, UAE.

IUCN, UNEP-WCMC, 2016. The World Database on Protected Areas (WDPA). www.protectedplanet.net/, last access: March 2017.

Jacobson, M., Delucchi, M., 2011. Providing all global energy with wind, water, and solar power, part i: Technologies, energy resources, quantities and areas of infrastructure, and materials. *Energy Policy* 39, 1154–1169.

Jacobson, M. Z., Archer, C. L., 2012. Saturation wind power potential and its implications for wind energy. *PNAS* 109 (39), 15679–15684.

Jacobson, M. Z., Delucchi, M. A., Bauer, Z. A. F., Savannah, C., Chapman, W. E., Cameron, M. A., Cedric, A., Chobadi, L., Erwin, J. R., Fobi, S. N., Owen, K., Harrison, S. H., Kwasnik, T. M., Lo, J., Yi, C. J., Morris, S. B., Moy, K. R., Neill, P. L. O., Redfern, S., Schucker, R., Sontag, M. A., Wang, J., Weiner, E., Yachanin, A. S., 2017. 100 % Clean and Renewable Wind , Water , and Sunlight (WWS) All- Sector Energy Roadmaps for 139 Countries of the World By 2050. *Joule* 1, 1–14.

Justus, C., et al., 1978. Methods for estimating wind speed frequency distributions. *Journal of Applied Meteorology* 17, 350–353.

- Keith, D., DeCarolis, J., Denkenberger, D., Lenschow, D. H., Malyshev, S., Pacala, S., Rasch, P., 2004. The influence of large-scale wind power on global climate. *PNAS* 101 (46), 16115–16120.
- Kielkiewicz, A., Marino, A., Vlachos, C., Maldonado, F., Lessis, I., 2015. The Practicality and Challenges of Using XL Monopiles for Offshore Wind Turbine Substructures. University of Strathclyde.
- Kleidon, A., 2010. Life, hierarchy, and the thermodynamic machinery of planet earth. *Physics of Life Reviews* 7, 424–460.
- Koppelaar, R., 2017. Solar-PV energy payback and net energy: Meta-assessment of study quality, reproducibility, and results harmonization. *Renewable and Sustainable Energy Reviews* 72, 1241–1255.
- Koppelaar, R., Koppelaar, H., 2016. The Ore Grade and Depth Influence on Copper Energy Inputs. *BioPhysical Economics and Resource Quality* 1 (2), 1–16.
- Kubiszewski, I., Cleveland, C. J., Endres, P. K., 2010. Meta-analysis of net energy return for wind power systems. *Renewable Energy* 35, 218–225.
- Lambert, J., Hall, C., Balogh, S., Gupta, A., Arnold, M., 2014. Energy, eroi and quality of life. *Energy Policy* 64, 153–167.
- Lamberterie, B. D., 2014. Steel production - energy efficiency working group. Tech. Rep. January, EUROFER.
- Lenzen, M., Munksgaard, J., 2002. Energy and CO₂ life-cycle analyses of wind turbinesreview and applications. *Renewable Energy* 26, 339–362.

Livaniou, S., Iordanis, S., Anaxagorou, P., Mocanu, B., Sykes, R., Goormachtigh, J., Christensen, J. M., Kristensen, J. T., Antrobus, M., 2015. Logistic Efficiencies And Naval architecture for Wind Installations with Novel Developments. Tech. Rep. 614020, Leanwind.

Lorenz, E., 1955. Available potential energy and the maintenance of the general circulation. *Tellus* 7, 271–281.

Lorenz, E., 1960. Generation of available potential energy and the intensity of the global circulation. *Dynamics of Climate*, Pergamon Press, Oxford, UK, 86–92.

Lu, X., McElroy, M. B., Kiviluoma, J., 2009. Global potential for wind-generated electricity. *PNAS* 106, 10933–10938.

Lunz, B., Stöcker, P., Eckstein, S., Nebel, A., Samadi, S., Erlach, B., Fischedick, M., Elsner, P., Sauer, D. U., 2016. Scenario-based comparative assessment of potential future electricity systems - A new methodological approach using Germany in 2050 as an example. *Applied Energy* 171, 555–580.

URL <http://dx.doi.org/10.1016/j.apenergy.2016.03.087>

Mackay, D. J., 2015. Sustainable Energy Without the Hot Air. UIT Cambridge.

Martinez, E., Sanz, F., Pellegrini, B., Jimenez, E., Blanco, J., 2009. Life cycle assessment of a multi-megawatt wind turbine. *Renewable Energy* 34, 667673.

- McGlade, C., Ekins, P., 2015. The geographical distribution of fossil fuels unused when limiting global warming to 2 degrees C. *Nature* 517 (7533), 187–190.
- Mediavilla, M., et al., 2013. The transition towards renewable energies: Physical limits and temporal conditions. *Energy Policy* 52, 297–311.
- Meyers, J., Meneveau, C., 2011. Optimal turbine spacing in fully developed wind-farm boundary layers. *Wind Energy* 15, 305–317.
- Miller, L., Brunsell, N., Mechem, D., Gans, F., Monaghan, A., Vautard, R., Keith, D., Kleidon, A., 2015. Two methods for estimating limits to large-scale wind power generation. *PNAS* 112, 11169–11174.
- Miller, L., Kleidon, A., 2016. Wind speed reductions by large-scale wind turbine deployments lower turbine efficiencies and set low generation limits. *PNAS* 113 (48), 13570–13575.
- Miller, L. M., Gans, F., Kleidon, A., 2011. Estimating maximum global land surface wind power extractability and associated climatic consequences. *Earth System Dynamics* 2, 1–11.
- Miller, L. M., Gans, F., Kleidon, A., 2012. The problem of the second wind turbine - a note on a common but flawed wind power estimation method. *Earth System Dynamics* 3, 79–86.
- Moriarty, P., Honnery, D., 2011. Is there an optimum level for renewable energy? *Energy Policy* 39, 2748–2753.

- Moriarty, P., Honnery, D., 2012. What is the global potential for renewable energy? *Renewable and sustainable energy reviews* 16, 144–252.
- Moriarty, P., Honnery, D., 2016. Can renewable energy power the future? *Energy Policy* 93, 3–7.
- Mulder, K., Hagens, N. J., 2008. Energy return on investment: Toward a consistency framework. *Ambio* 37, 74–79.
- Murphy, D. J., 2014. The implications of the declining energy return on investment of oil production. *Phil. Trans. R. Soc. A* 372 (20130126).
- Murphy, D. J., Hall, C. A., 2011. Energy return on investment, peak oil, and the end of economic growth. *Ann. N.Y. Acad. Sci.* 1219, 52–72.
- Murphy, D. J., Hall, C. A., Dale, M., Cleveland, C., 2011. Order from chaos : A preliminary protocol for determining the eroi of fuels. *Sustainability* 3, 1888–1907.
- NASA, 2009. Distance to the nearest coast. <https://oceancolor.gsfc.nasa.gov/docs/distfromcoast/>, last access: March 2017.
- Nylund, N.-O., Erkkilä, K., 2005. Heavy-duty truck emission and fuel consumption: Simulating real-world driving in laboratory conditions. In: Proceeding of the 2005 DEER conference. pp. 1–23.
- Peixoto, J. P., Oort, A. H., 1992. Physics of climate. American Institute of Physics, Springer-Verlag, New York, USA.

- Pereg, J. R. M., Fernandez de la Hoz, J., 2013. Life cycle assessment of 1kWh generated by a wind farm Gamesa G90-2.0 MW onshore. Tech. rep., GAMESA.
- Raugei, M., 2016. Methodological Guidelines on Net Energy Analysis of Photovoltaic Electricity. Tech. Rep. IEA-PVPS T12-07, International Energy Agency.
- Sharpe, B., Muncrief, R., 2015. Literature Review : Real-World Fuel Consumption of Heavy-Duty Vehicles in the United States , China , and the European Union. Tech. rep., ICCT.
- Smith, A., Stehly, T., Musial, W., 2015. 2014-2015 offshore wind technologies market report. Tech. Rep. NREL/TP-5000-64283, National Renewable Energy Laboratory.
- Snieckus, D., March 2017. French wind lobbying for 2GW floating tender early next year.
- Statoil, 2015. Hywind Scotland Pilot Park - Environmental Statement. Tech. rep., Statoil.
- Stevens, R., Dennice, F., Meneveau, C., 2016. Effects of turbine spacing on the power output of extended wind farms. Wind Energy 19, 359–370.
- Stevens, R., Meneveau, C., 2017. Flow structure and turbulence in wind farms. Annu. Rev. Fluid Mech. 49, 311–339.
- Templin, R. J., 1974. An Estimate of the Interaction of Windmills in

Widespread Arrays. Tech. rep., Rep. N.A.E. LTR-LA-171, National Research Council of Canada, Ottawa.

The Crown Estate, 2016. Offshore wind operational report. Tech. rep., The Crown Estate, last Access: June 2017.

Tian-Pau, C., Feng-Jiao, L., Hong-Hsi, K., Shih-Ping, C., Li-Chung, S., Shye-Chorng, K., 2014. Comparative analysis on power curve models of wind turbine generator in estimating capacity factor. Energy 73, 88–95.

Tremeac, B., Meunier, F., 2009. Life cylce analysis of 4.5 mw and 250 w wind turbines. Renewable and Sustainable Energy Reviews 13, 2104–2110.

VLIZ, 2014. Union of the ESRI Country shapefile and the Exclusive Economic Zones (version 2). <http://www.marineregions.org/>, last access: April 2017.

Walmsley, M. R., Walmsley, T. G., Atkins, M. J., Kamp, P. J., Neale, J. R., 2014. Minimising carbon emissions and energy expended for electricity generation in New Zealand through to 2050. Applied Energy 135, 656–665.

URL <http://dx.doi.org/10.1016/j.apenergy.2014.04.048>

WEC, 2016. World Energy Scenarios. Tech. rep., World Energy Concil.

WWF, 2011. The energy report 100 % renewable by 2050. Tech. rep., WWF.

Zou, P., Chen, Q., Yu, Y., Xia, Q., Kang, C., 2017. Electricity markets evolution with the changing generation mix: An empirical analysis based on China 2050 High Renewable Energy Penetration Roadmap. Applied

Energy 185 (2011), 56–67.

URL <http://dx.doi.org/10.1016/j.apenergy.2016.10.061>